JOURNAL OF MATERIALS SCIENCE **36** (2001) 2721 – 2741

Precipitation hardening of Cu-Fe-Cr alloys

Part II *Microstructural characterisation*

H. FERNEE, J. NAIRN, A. ATRENS
Department of Mining Minerals and Materials Engineering, The University of Queensland, Brisbane Qld Australia 4072
E-mail: altrens@minmet.uq.oz.au.

This research is part of a project whose scope was to investigate the engineering properties of new non-commercial alloy formulations based on the Cu rich corner of the Cu-Fe-Cr ternary system with the primary aim of exploring the development of a new cost-effective high-strength, high-conductivity copper alloy. Promising properties have been measured for the following alloys: Cu-0.7wt%Cr-0.3wt%Fe and Cu-0.7wt%Cr-2.0wt%Fe. This paper reports on the microstructural characterisation of these alloys and discusses the mechanical and electrical properties of these alloys in terms of their microstructure, particularly the formation of precipitates. These alloys have evinced properties that warrant further investigation. Cost modelling has shown that Cu-0.7wt%Cr-0.3wt%Fe is approximately 25% cheaper to produce than commercial Cu-1%Cr. It has also been shown to be more cost efficient on a yield stress and % IACS per dollar basis. The reason for the cost saving is that the Cu-0.7%Cr-0.3%Fe alloy can be made with low carbon ferro-chrome additions as the source of chromium rather than the more expensive Cu-Cr master-alloy. For applications in which cost is one of the primary materials selection criteria, it is envisaged that there would be numerous applications in both cast and wrought form, where the Cu-0.7%Cr-0.3%Fe alloy would be more suitable than Cu-1%Cr.

1. Introduction

This is the second paper describing research aimed at developing new high-strength high-conductivity copper alloys based on the copper rich part of the Cu-Fe-Cr phase diagram. The first paper [1] reported promising mechanical properties for the alloy Cu-0.7%Cr-0.3%Fe. This paper reports the microstructural characterisation which was carried out to understand this alloy.

2. Experimental

Microstructural characterisation of the alloys was carried out using a wide variety of different techniques in order to be able to interpret and explain the properties.

2.1. Preparation of metallographic samples

Metallographic samples were mounted in a two component epoxy resin known as Epothin using one inch diameter moulds. Mounted specimens were degassed prior to resin setting in order to remove any air bubbles from the mould. Grinding of metallographic specimens was done in five stages using 120, 200, 420, 600 and 1200 grit SiC paper. Polishing was done in 3 stages, using commercial metal polishes Brasso and Silvo, and finally 0.05 micron gamma alumina powder. For Silvo velvet cloth was used, for Brasso selvet cloth, while for alumina a Buehler short nap microcloth was used. To achieve a good quality polish very long polishing times were required using the alumina. It was found that the scratches were removed considerably faster if the specimens were lightly etched with alcoholic ferric chloride prior to polishing with alumina. Specimens prepared in this way were used for analysis with optical microscopy, SEM and WDS.

2.2. Optical microscopy

The microstructures were examined with a Reichert-Jung Polyvar-Met optical microscope. Best observation conditions were dependent on individual samples but in most cases samples were viewed unetched using normal reflected light. Light etching with alcoholic ferric chloride was used to observe grain boundaries. For grain size measurements polarised light in dark field conditions was used to improve contrast.

2.3. Scanning electron microscopy

Microstructures were further examined using JEOL 6400F and JEOL 820 scanning electron microscopes in composition and secondary electron image mode. An acceleration voltage of 20 kV was used in most cases. To prevent charging of the specimens (because they were mounted in insulating epoxy) colloidal graphite was painted between the sample (mounted in the epoxy) and the specimen holder.

2.4. Wavelength dispersive spectroscopy

Wavelength Dispersive Spectroscopy (WDS) was used to obtain quantitative information about the composition of each alloy. A JEOL JXA-8800L Electron Probe Microanalyser equipped with a Link Ge EDS spectrometer, was used with an accelerating voltage of 20 kV and a probe current of 15 nA. The Microanalyser has four wave length dispersive spectrometers. Prior to quantitative analysis it was necessary to calibrate each wave length dispersive spectrometer using standards from the Charles Taylor Block. The PRZ correction method supplied by JEOL was used to obtain quantitative results. As for SEM specimens colloidal graphite was required to be painted between the sample and the specimen holder to earth any build up of charge. Even when using colloidal graphite some charging of the specimens was still observed. A thin carbon coating prior to analysis was found to prevent this. Carbon coating of all specimens was carried out using a JEOL Carbon Coater. It should be noted that the standards used were also carbon coated.

In order to ensure that accurate results were produced the standards in the Charles Taylor Block were run as unknowns prior to analysing alloys. If the total calculated weight % of each standard was not within 0.3% of 100%, then the standards were retested. Analyses of alloys were only accepted if the total calculated wt% was between 98.5 and 101.5 wt%. A minimum of five analyses, usually eight were averaged to determine the composition of each alloy. All acceptable analyses were normalised prior to averaging. The concentration of trace additions in some alloys could not be determined due to overlap of peaks.

Wavelength Dispersive Spectroscopy was used to determine the concentration of alloying elements within the copper matrix of alloys in the solution treated condition. The composition of secondary and primary precipitates could not be accurately measured because of their small size in comparison to that of the interaction volume from which signal was produced. Similarly the concentration of alloying elements within the matrix of aged alloys could not be determined due to fine secondary precipitates contained within the interaction volume affecting the results.

The microanalyser was also equipped with an EDS detector. This was used to analyse the composition of the primary and secondary precipitates of the ternary Cu-Fe-Cr alloys. All analyses were carried out in a single session using an accelerating voltage of 10 kV and a probe current of 50 nA. This lower accelerating voltage was still able to excite both Fe and Cr Kα radiation, however the size of the interaction volume was small which meant that the smaller secondary precipitates could be analysed more accurately. These spectra could be used to quantitatively compare the ratios of Fe to Cr in the different precipitates and alloys investigated.

2.5. Transmission electron microscopy

Transmission electron microscopy (TEM) was used to study the size and crystal structure of secondary precipitates in the three ternary Cu-Fe-Cr alloys. The nature of the precipitate-matrix interface was also investigated as was their orientation in the matrix. Each alloy was investigated in the peak aged condition. The evolution of the Cu-0.7wt%Cr-0.3wt%Fe alloys microstructure with aging was also investigated.

All analyses were carried out using a JEOL 4000 FX analytical electron microscope. The accelerating voltage used was 400 kV. The microscope has an image resolution of 0.23 nm and a maximum magnification of 800 000 times. The image can be further magnified by 20 times by video for viewing purposes. The microscope contains a Ge energy dispersive spectrometer (EDS) for selected area compositional analysis. A Gatan double-tilt holder was used for tilting the specimen to obtain the desired zone axis. Analysis in bright and dark field was carried out although bright field analysis was more successful. Selected area diffraction patterns were also taken. In most cases the maximum magnification used was 250 000 times. However for high resolution imaging 800 000 times was used.

Specimens for investigation were prepared from hardness blocks that had previously been heat treated and used for hardness testing. Thin slices (thicknesses $\sim$400 μm) were cut from the hardness blocks with a Buehler Isomet low speed diamond saw. 3 mm diameter discs were punched out of the slices and then ground down to 100 μm using 1000 grit SiC paper. The discs were electropolished using a Struers Tenupol-3 twin jet electropolisher in 45 vol% orthophoshoric acid in water at 12 V and temperature $\sim$23°C (room temp). The sensor that detects when perforation of the specimen occurs was set to its most sensitive setting. After electropolishing the specimens were washed sequentially in three glass beakers of ethanol, dried on inert filter paper and stored under vacuum to prevent oxidation prior to analysis.

Specimens prepared in this manner where suitable for low resolution electron microscopy up to a magnification of $\sim$250 000 times. However the size of the thin section surrounding the perforation, from which images could be obtained, was quite small. For high resolution imaging, specimens with a larger thin section were necessary. Ion Beam Thinning was used to increase the size of the thin section of some specimens. A Gatan 600 Duo-mill was used. The thinning was done in two stages, the first for 30 minutes at 5 kV with an 8° glancing angle. This was followed by 15 minutes at 3 kV. The low voltage was used to minimise damage to the specimen. All thinning was carried out with liquid nitrogen cooling. After thinning, specimens were allowed to warm to room temperature and then within 15 minutes were taken and examined in the TEM. This ensured that no oxide film was present on the samples. This method was found to produce specimens with large thin sections suitable for high resolution analysis.

Imaging of precipitates in TEM was performed with the beam direction, B, very close to Cu [1, 0, 0] direction. Conventional imaging was performed using a small objective aperture that surrounded the direct beam. High resolution multi-beam images were obtained using a larger objective aperture that just allowed

Cu (0, 2, 2), (0,$\bar{2}$, $\bar{2}$), (0, $\bar{2}$, 2) and (0, 2, $\bar{2}$) reflections to pass.

2.6. X-Ray diffraction

X-Ray Diffraction (XRD) was used to analyse the precipitation reaction of the ternary Cu-0.7wt%Cr-0.3wt%Fe alloy. Analyses were carried out using a Phillips X-ray generator (model – PW1130) equipped with a Bragg-Brentano type goniometer (model – PW1050). Samples used were hardness blocks that had been ground with 1000 grit SiC paper. These were mounted using plasticine into specimen holders. X-rays were generated using a copper tube to produce copper Kα radiation with a wavelength of 1.54 angstroms and an energy of 8.03 keV. The X-rays were passed through a graphite monochromator. The diffractometer was controlled using Sietronics Sie112 software set for step scan. The diffractometer was set at a scan speed of 0.07 degrees per minute, an operating voltage of 40 kV and current of 40 mA. Scans were carried out from 35 through to 85 degrees 2θ. The background was calculated using a Sietronics Sie112 trace analyser and subtracted from all scans.

3. Results

3.1. Optical microscopy

Optical microscopy showed that the microstructure of the three Cu-Fe-Cr alloys were dendritic, Figs 1 and 2. Dendrites were surrounded by a rod like eutectic of copper and a coarse second phase. There were fine secondary precipitates in the dendrite arms of the as-cast alloys which dissolved during solution treatment and could not be seen optically even after extended ageing. Solution treatment did not dissolve all the eutectic phase, Fig. 2. The grain size of AC alloys was large and would have negligible influence upon the strength or electrical conductivity.

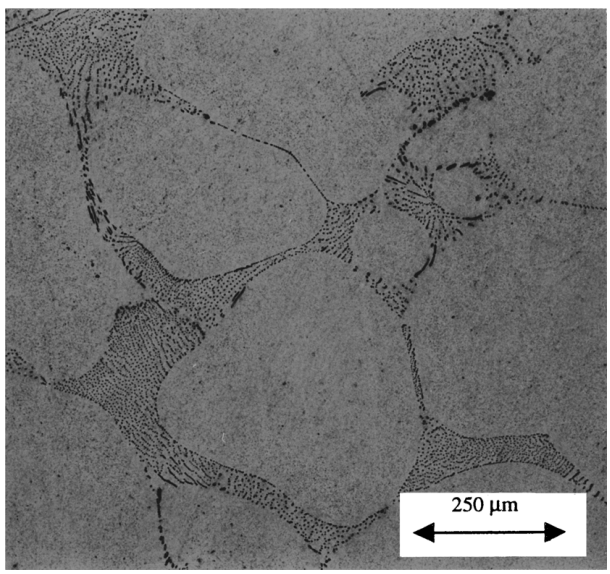

Figure 1 Optical micrograph of as-cast Cu-0.7%Cr-2.0%Fe alloy showing dendritic microstructure surrounded by rod like eutectic. Unetched.

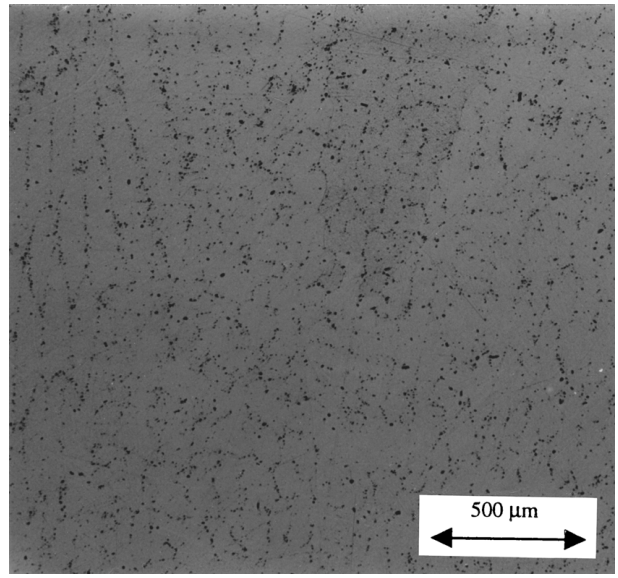

Figure 2 Optical micrograph of solution treated Cu-0.7%Cr-0.8%Fe alloy showing eutectic still present. Unetched.

3.2. Scanning electron microscopy

Samples of the alloys were examined using a Jeol 820 and 6400 SEM in both compositional and secondary electron mode. Samples were examined in as-cast (AC), solution treated and various aged conditions. Samples were etched in alcoholic ferric chloride and Energy dispersive X-ray spectroscopy (EDS) was carried out to explore chemical composition. The Scanning Electron Microscopy (SEM) confirmed the results of the optical microscopy. In particular, there was no evidence of secondary precipitates in the three Cu-Fe-Cr alloys after solution heat treatment.

3.3. Energy dispersive X-ray spectroscopy

Energy dispersive x-ray spectroscopy (EDS) was carried out on the second phase in the eutectic and on the secondary precipitates of the three Cu-Fe-Cr alloys in different heat treated conditions. All EDS was carried out in the same session using an accelerating voltage of 10 kV. A low accelerating voltage was used in order to minimise the size of the interaction volume from which signal was produced.

The EDS suggests that the second phase in the eutectic and the secondary precipitates in the three AC Cu-Fe-Cr alloys contained both Fe and Cr. For each of the alloys, the primary precipitates in the eutectic phase were predominantly made up of Cr however the ratio of Fe to Cr (judging from the peak heights) in each alloy varied. This is illustrated in Figs 3 to 5 which show EDS spectra of primary precipitates in each alloy. It can be seen from the intensity of the Fe peaks that the Fe content of the Cr rich eutectic phase increased with increasing Fe content of the alloy.

Analysis of secondary precipitates in the AC alloys showed that the ratio of Fe to Cr in the secondary precipitates was different for each alloy and was different from that in the Cr rich eutectic phase. The amount of Fe in secondary precipitates was much higher. As for the Cr rich eutectic phase, the amount of Fe in the

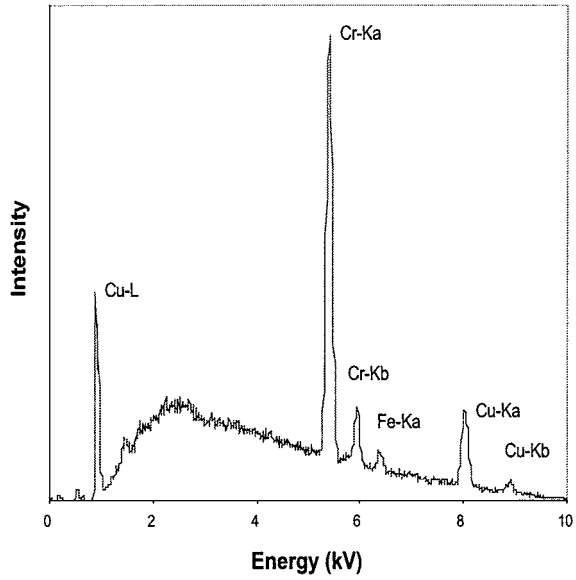

Figure 3 EDS spectra of Cr rich eutectic phase in as-cast Cu-0.7%Cr-0.3%Fe alloy. 10 kV.

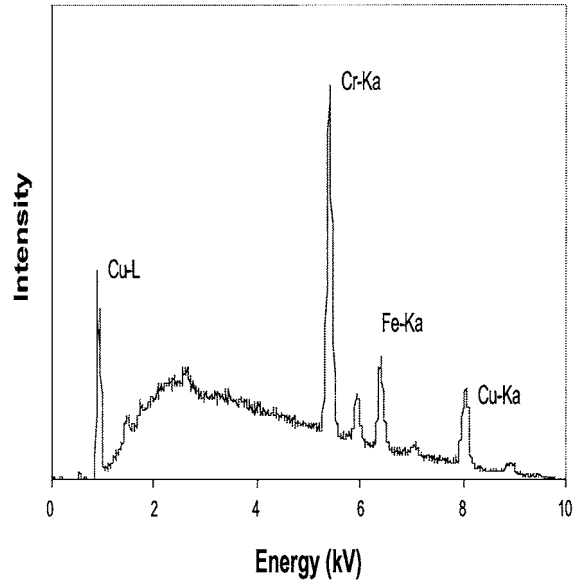

Figure 5 EDS spectra of Cr rich eutectic phase in as cast Cu-0.7%Cr-2.0%Fe alloy. 10 kV.

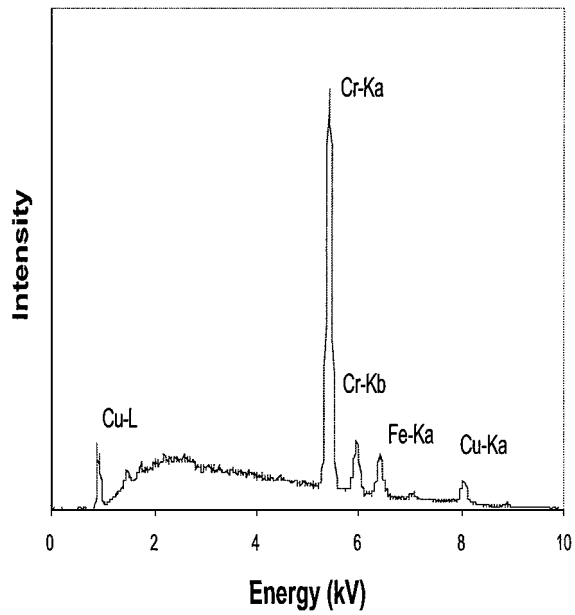

Figure 4 EDS spectra of Cr rich eutectic phase in as cast Cu-0.7%Cr-0.8%Fe alloy. 10 kV.

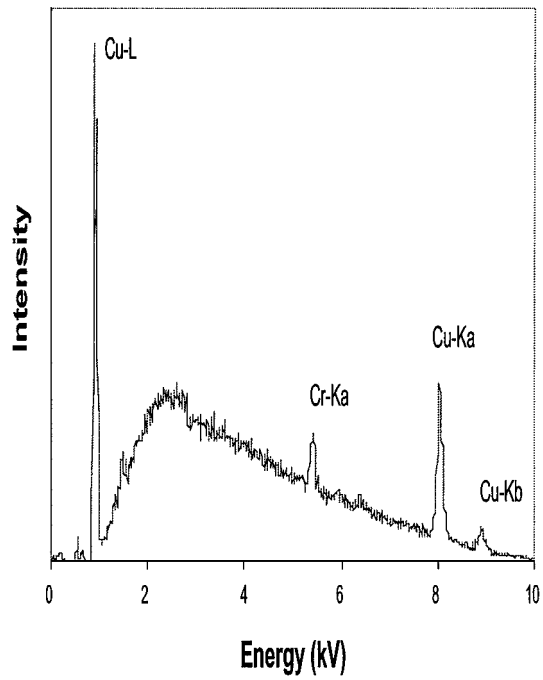

Figure 6 EDS spectra of secondary precipitate in as-cast Cu-0.7%Cr-0.3%Fe alloy. 10 kV.

secondary precipitates increased with increasing Fe in the alloy. The smaller size of secondary precipitates meant that the relative size of the Cu peaks were significantly larger and the Fe and Cr peaks significantly smaller due to more signal being produced from the matrix. EDS spectra of secondary precipitates for each of the Cu-Fe-Cr alloys are shown in Figs 6 to 8.

Spectra were also taken of the matrix of the AC alloys. Fig. 9 shows the EDS spectra of the matrix of Alloy C. A very small Fe peak was visible. No evidence of Cr peaks were observed in this spectra or in spectra taken from the matrix of the other alloys. An Fe peak was only observed in the spectra of Alloy C. Based upon this it was apparent that any signal collected from the matrix would not contribute significantly to the Fe and Cr peaks recorded for the precipitates. The matrix and Cr rich eutectic phase of each alloy were examined in solution treated and overaged condition. No change in the spectra was observed for any alloy.

3.4. Wavelength dispersive spectroscopy

Wavelength Dispersive Spectroscopy (WDS) was used to quantitatively determine the concentration of Fe and Cr in the matrix of the alloys. This information was used to determine the volume fraction of second phase precipitates that were responsible for precipitation hardening. Similar quantitative analysis of the composition of the eutectic and secondary precipitates was not possible due to their small relative size.

The same samples used in optical microscopy were used in the WDS investigations. In order to ensure

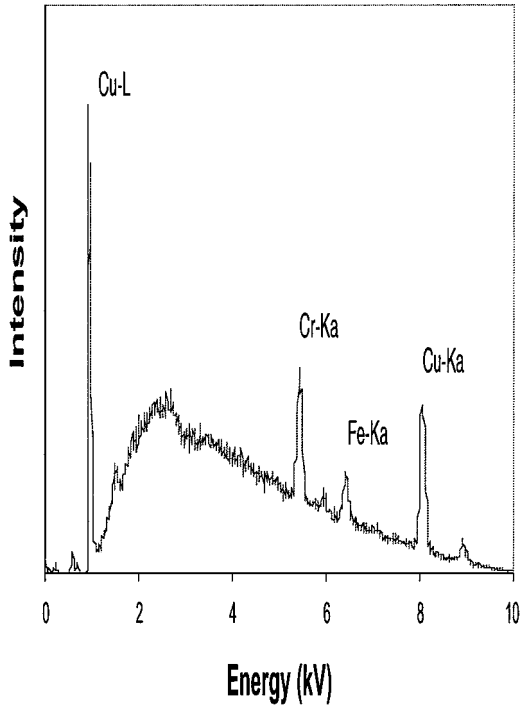

Figure 7 EDS spectra of secondary precipitate in as cast Cu-0.7%Cr-0.8%Fe alloy. 10 kV.

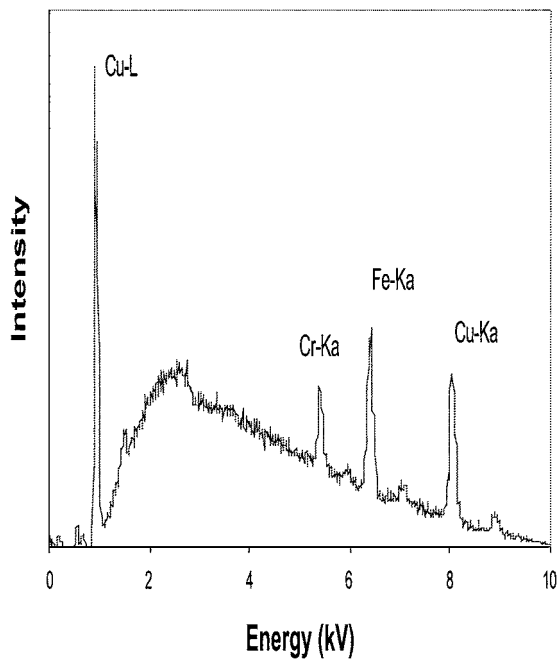

Figure 8 EDS spectra of secondary precipitate in as cast Cu-0.7%Cr-2.0%Fe alloy. 10 kV.

the average compositions were as accurate as possible, measurements were taken from as widely spaced positions as possible on a number of samples. For each measurement care was taken to avoid any primary precipitate being in the interaction volume. As a precautionary measure, measurements were only accepted if the total weight percent of copper and alloying elements added to between 98.5 and 101.5 wt%. A minimum of five measurements, were used to determine the average composition of each sample. All measurements were normalised before being averaged. In all cases scatter was minimal.

TABLE I Concentration of Cr in solid solution at different locations within the solution treated Cu-1%Cr casting

Position in Casting	wt% Cr
Top	0.57
Middle	0.58
Bottom	0.59
Outer Edge	0.58

TABLE II Concentration of alloying elements in the matrix of the alloys after solution treatment at 1050°C for two hours

Alloy	wt% Cr	wt% Fe
Cu-0.7%Cr-0.3%Fe (Alloy A)	0.55	0.26
Cu-0.7%Cr-0.8%Fe (Alloy B)	0.51	0.78
Cu-0.7%Cr-2.0%Fe (Alloy C)	0.40	1.60
Cu-1%Cr (Alloy Z)	0.58	—
Cu-1%Fe (Alloy Y)	—	1.05

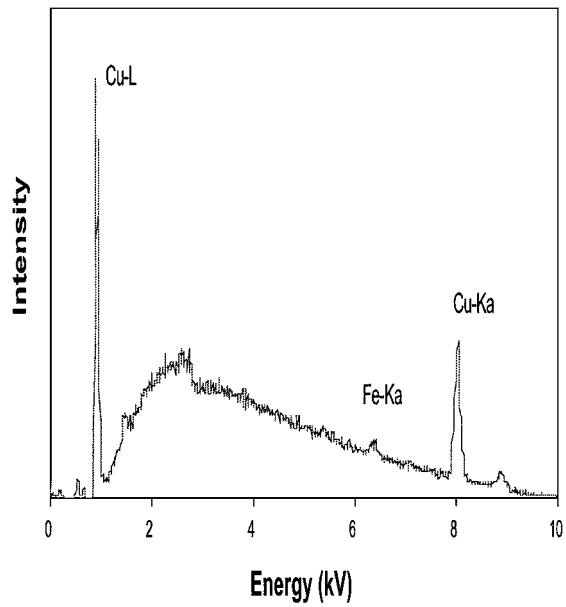

Figure 9 EDS spectra of matrix of as-cast Cu-0.7%Cr-2.0%Fe alloy. 10 kV.

Additional tests were carried out on solution treated samples to determine if the concentration of alloying elements was affected by where in the casting samples had come from, ie. centre, edge, top or bottom. These results are shown in Table I. It is apparent that the concentration of alloying elements in the matrix of solution treated samples was uniform.

The concentration of alloying elements in the matrix of all alloys after solution treatment are shown in Table II. For Alloy A and Alloy C it is apparent that some dissolution of primary precipitates had occurred as the concentration of alloying elements in solid solution had increased from that measured in the AC condition.

For the solution treated Alloy Y, all alloying additions were dissolved in the copper matrix. This was as expected based upon micrographs of solution treated samples which showed no evidence of primary precipitates. For Alloy Z, 0.58 wt% Cr was dissolved in solid

solution. This is significantly less than the maximum solubility of 0.73 wt% at 1076°C reported in the literature [2], however the solubility of Cr in Cu is very dependant upon temperature and decreases rapidly with decreasing temperature. 0.58 wt% is consistent with the maximum solubility at 1050°C. For the solution treated ternary Cu-Fe-Cr alloys, the solubility of Cr decreased with increasing Fe content of the alloy. Similarly the solid solubility of Fe was also decreased by Cr in solid solution. The maximum solubility of Fe in Cu is 4.1 wt% [2] and the solubility does not decrease as rapidly with temperature as for Cu-Cr. At 1050°C the solubility of Fe in Cu for binary alloys is well in excess of 3 wt%. Based upon this it would be expected that more than 1.6 wt% Fe would be in solid solution for the solution treated Alloy C unless Cr was decreasing the solubility of Fe.

The concentration of alloying elements in the matrix of overaged samples of four of the five alloys were investigated. Contrary to expectations the measured weight percent of Fe and Cr in the matrix of each overaged sample were within 0.01 wt% of those measured for the solution treated samples. The reason for this was that secondary precipitates that had formed during aging were of the order of a few nm. This fine dispersion of precipitates would be included in the interaction volume of the electron probe whose diameter is of the order of μm. Therefore the actual concentration of alloying elements in the interaction volume from which the signal was produced had remained unchanged. As a result WDS could not be used to measure the concentration of alloying elements in solid solution in aged samples. The fact that the weight percent of alloying elements measured in different samples were almost identical was further evidence that after solution treatment, the concentration of alloying elements in the matrix was uniform throughout the castings.

3.5. X-ray diffraction

X-ray diffraction (XRD) was carried out on samples of the Cu-0.7%Cr-0.3%Fe alloy (Alloy A) in various aged conditions to explore the efficacy of this technique in providing information about the precipitate crystal structure. The scans obtained from a solution treated specimen of Alloy A contained only large peaks due to copper.

Scans carried out on peak aged and underaged samples did not show evidence of additional peaks. This was attributed to the precipitates being too small and their volume fraction too low. Scans on samples which had been aged for 24 hours at 500°C showed a number of very small additional peaks. The position of these peaks was equivalent to where peaks would be expected for both body centred cubic (bcc) Fe and Cr. Diffraction peaks for both bcc Fe and Cr are in almost identical positions [3]. The position of the peaks suggest that the precipitates in the overaged sample were bcc.

3.6. Transmission electron microscopy

Transmission Electron Microscopy (TEM) was carried out on specimens of Alloy A in various heat treated conditions and on peak aged specimens of Alloy B and Alloy C. The purpose of the investigation was to seek information about the precipitates and the precipitation reaction. This information was used to interpret the observed precipitation hardening behaviour of each alloy. Most investigations were carried out at magnifications of up to 300,000 times. Some high resolution lattice imaging was carried out at magnifications of up to 800,000 times on peak aged Alloy A.

3.6.1. Solution treated Cu-0.7%Cr-0.3%Fe

Bright and dark field images of solution treated Alloy A at magnifications of up to 300,000 times showed evidence of the presence of some precipitates. Fig. 10 shows a bright field image of the solution treated matrix where a few very small precipitates can be seen. A diffraction pattern taken from the matrix is shown in Fig. 11. It shows a [1, 0, 0] diffraction pattern typical for a fcc crystal such as copper. Additional diffraction spots due to the presence of precipitates can not be seen. Some elongation of the diffraction spots along the $\langle 2, 0, 0 \rangle$ direction has occurred. This was attributed to ordering within the matrix or the presence of coherent GP zones.

3.6.2. Under-aged Cu-0.7%Cr-0.3%Fe

Examination of samples that had been aged for 5 minutes at 500°C showed that considerable precipitation had occurred, as illustrated in Fig. 12.

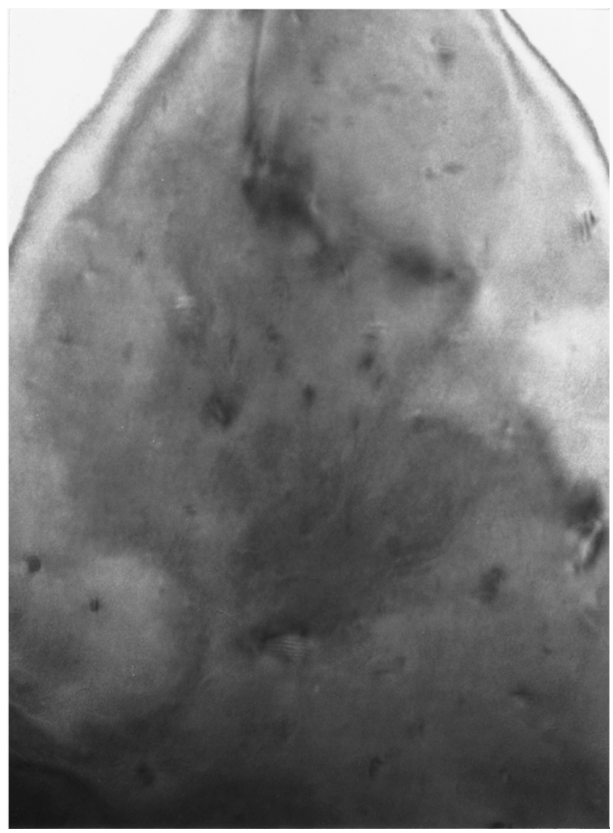

Figure 10 TEM bright field image of solution treated Cu-0.7%Cr-0.3%Fe alloy showing matrix almost precipitate free. Beam direction B = [1, 0, 0] 200 k.

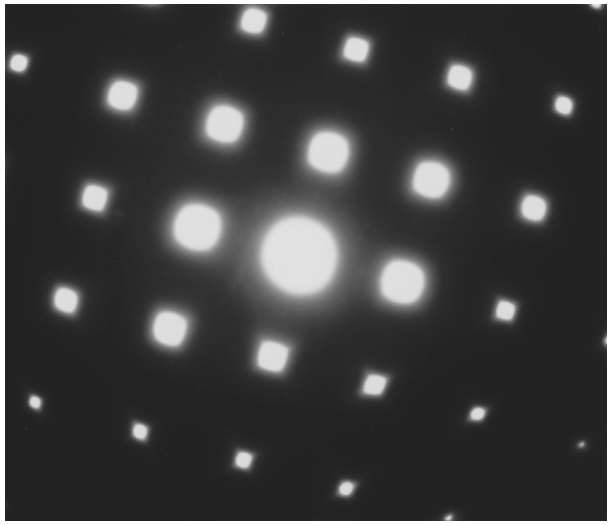

Figure 11 Diffraction pattern form solution treated Cu-0.7%Cr-0.3%Fe alloy showing typical fcc diffraction pattern. Some distortion of reflections has occurred indicating ordering or coherent precipitates in matrix. Beam direction B = [1, 0, 0].

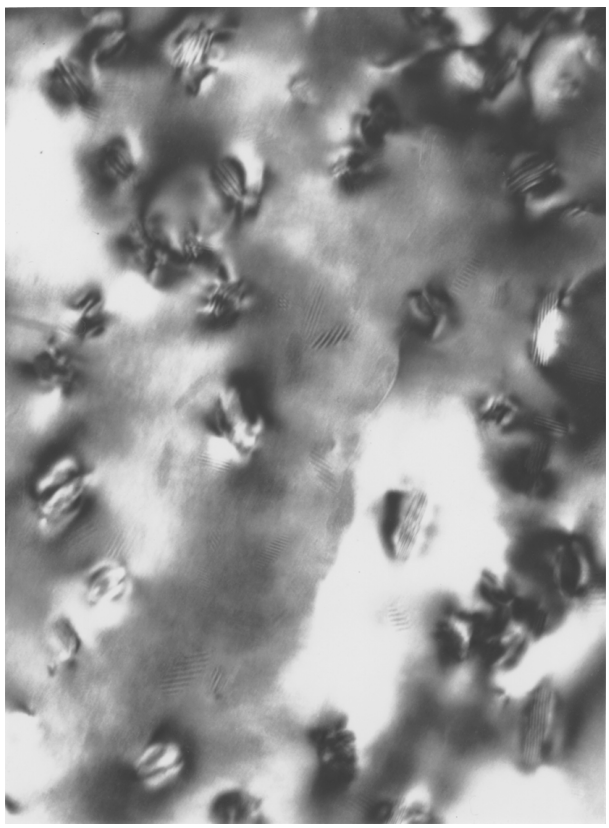

Figure 12 TEM bright field image of Cu-0.7%Cr-0.3%Fe alloy aged for 5 minutes at 500°C. Precipitates are clearly visible. Beam direction B = [1, 0, 0]. 200 k.

Precipitates could be seen randomly dispersed in the matrix and were ∼5–20 nm long. The average size appeared to be around 10 nm. Diffraction patterns taken from samples aged for 5 minutes contain semi-continuous rings as seen in Fig. 13. These rings indicated that the precipitates were randomly oriented within the matrix and therefore incoherent with the matrix.

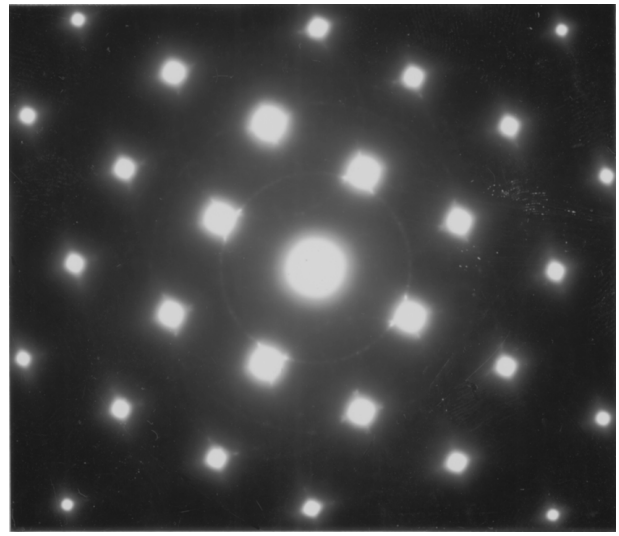

Figure 13 Diffraction pattern of Cu-0.7%Cr-0.3%Fe alloy aged for 5 minutes. Rings due to randomly oriented precipitates are visible. Beam direction B = [1, 0, 0].

3.6.3. Peak-aged Cu-0.7%Cr-0.3%Fe

The microstructure of the peak aged Alloy A is shown by the bright field images in Figs 14 and 15. Fig. 14 showed a high concentration of precipitates randomly distributed in the matrix. Fig. 15 showed that the precipitates were 10–20 nm long, the average length ∼15 nm. Precipitates appeared to be thick rods. The precipitates had not grown significantly. It was not possible to tell from the bright field images whether the volume fraction of precipitates had increased compared to that in the sample aged for 5 minutes. A diffraction pattern taken from the peak aged alloy is shown in

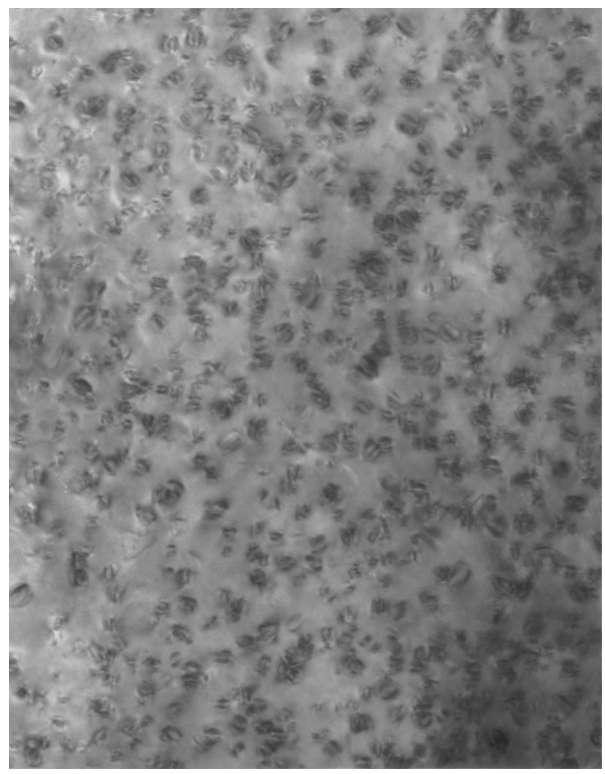

Figure 14 TEM bright field image of peak aged Cu-0.7%Cr-0.3%Fe alloy showing peak aged precipitates. Beam direction B = [1, 0, 0]. 50 k.

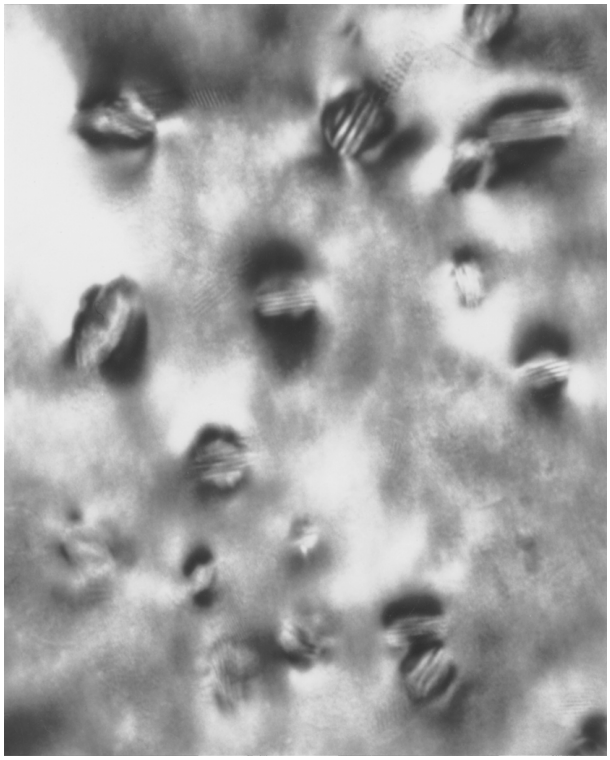

Figure 15 TEM bright field image of peak aged Cu-0.7%Cr-0.3%Fe alloy showing precipitates to be between 10–20 nm in length. Beam direction B = [1, 0, 0]. 300 k.

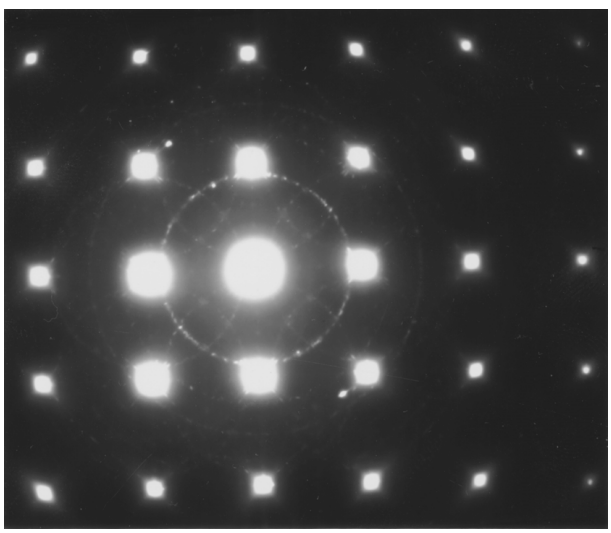

Figure 16 Diffraction pattern of peak aged Cu-0.7%C-0.3%Fe alloy. Rings are visible as are faint ordered reflections surrounding fcc copper matrix reflections. Beam direction B = [1, 0, 0].

Fig. 16. Diffraction rings were more pronounced than in the specimen aged for 5 minutes. This indicated a greater concentration of randomly oriented incoherent precipitates. Indexing of rings showed that the precipitates were bcc. This supported the results obtained from XRD. The positions and intensities of rings were the same as those that would be produced by both bcc Fe and Cr precipitates, which give almost identical diffraction patterns. Close examination of Fig. 16 reveals small reflections arranged periodically around the large matrix reflections. One such reflection has been highlighted. They are shown clearly in the slightly over exposed diffraction pattern shown in Fig. 17. Similarly

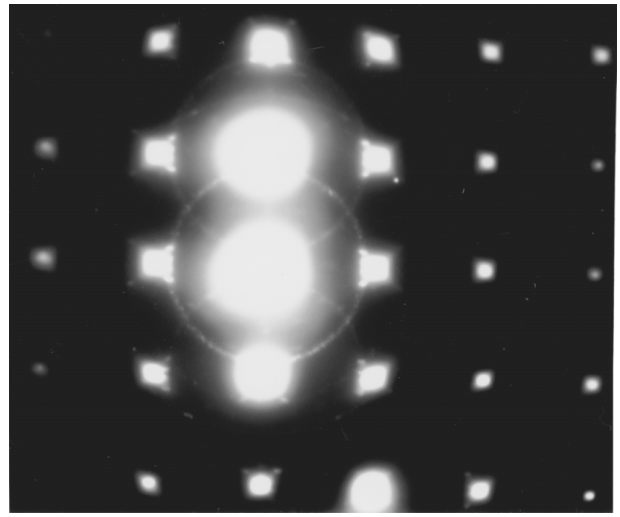

Figure 17 Diffraction pattern of peak aged Cu-0.7%C-0.3%Fe alloy that has been slightly over exposed. Ordered reflections surrounding fcc copper reflections are visible. Beam direction B = [1, 0, 0].

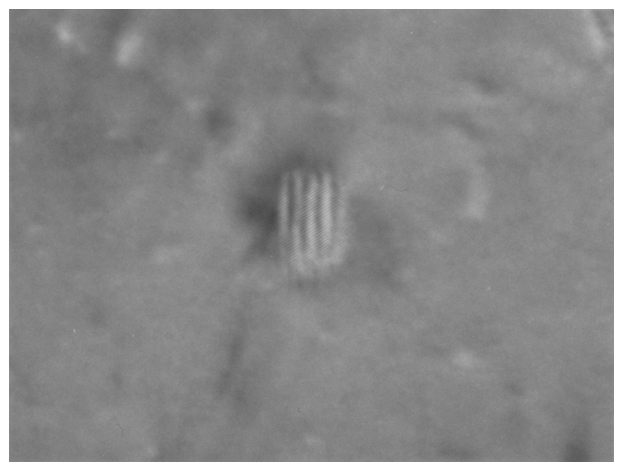

Figure 18 High resolution lattice image of precipitate in peak aged Cu-0.7%Cr-0.3%Fe alloy. The precipitate appears to be coherent with the copper lattice. Beam direction B = [1, 0, 0]. 800 k.

they can be seen in the diffraction pattern taken from the specimen aged for 5 minutes. These ordered reflections indicated that some of the precipitates were preferentially oriented in the matrix indicating some degree of coherency.

High resolution TEM was carried out on samples of the peak aged Alloy A at magnifications of 800,000×. Some of the precipitates were found to be partially coherent with the parent Cu lattice. Fig. 18 shows a micrograph of a partially coherent secondary precipitate which has been marked, (2, 0, 0) planes visible in the copper matrix appear continuous through the precipitates indicating coherency. Precipitates whose interfaces with the matrix appeared incoherent could not be imaged under these lattice imaging conditions. Such partially coherent precipitates seem to relate to those faint but ordered reflections rather than the diffractions rings.

Fourier transformation produced diffraction patterns were obtained from high resolution lattice images. A diffraction pattern obtained from the micrograph in Fig. 18 is shown in Fig. 19. Calculations were carried

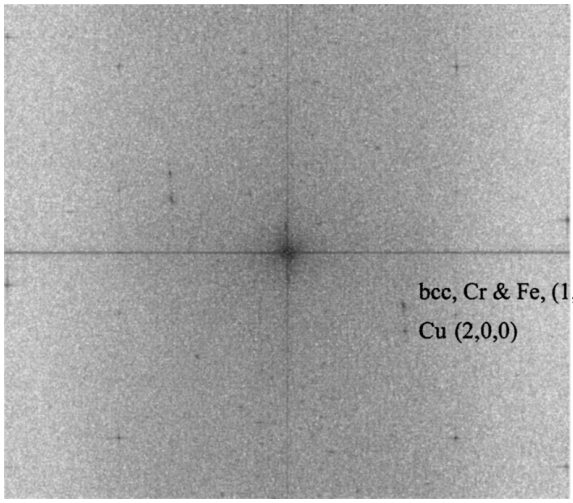

Figure 19 Diffraction pattern of precipitate shown in Fig. 18. Spots indexed have been labelled.

out to index the spots based upon the knowledge that the (2, 0, 0) planes in the copper matrix were being imaged. The lattice spacing of the planes visible in the precipitate were 2.02 angstroms. This was equivalent to the lattice spacing for (1, 1, 0) planes of both bcc Fe and Cr. The position of these reflections relative to the Cu (2, 0, 0) in the diffraction pattern is the same as those spots in the diffraction pattern that were produced by the precipitate. This indicates that the ordered reflections seen in the diffraction pattern are being produced by the partially coherent precipitates seen in the high resolution images.

The diffraction pattern shown in Fig. 19 was filtered for background noise and inverse Fourier transform was performed to obtain the clearer image of the precipitate shown in Fig. 20. The lattice image of the precipitate in the enhanced image appears coherent with the copper matrix.

3.6.4. Over-aged Cu-0.7%Cr-0.3%Fe

Examination of overaged samples that had been aged for 12 hours at 500°C showed that the precipitates were 10–20 nm long and randomly distributed within the matrix. Precipitates were not noticeably bigger than those in the peak aged specimen. A diffraction pattern taken from the sample is shown in Fig. 21. Diffraction rings were still visible however they were not as clear nor as continuous as those in the peak aged sample. This indicated that the precipitates within the matrix had coarsened and the total number had decreased during aging. Ordered reflections could still be made out in the diffraction pattern indicating some partially coherent precipitates were still present. Diffraction spots in Fig. 21 were still elongated along the ⟨2, 2, 0⟩ direction. The elongation of diffraction spots, observed for specimens in all aged conditions, was unlikely to have been caused by precipitates. Some form of ordering within the matrix was thought to be responsible.

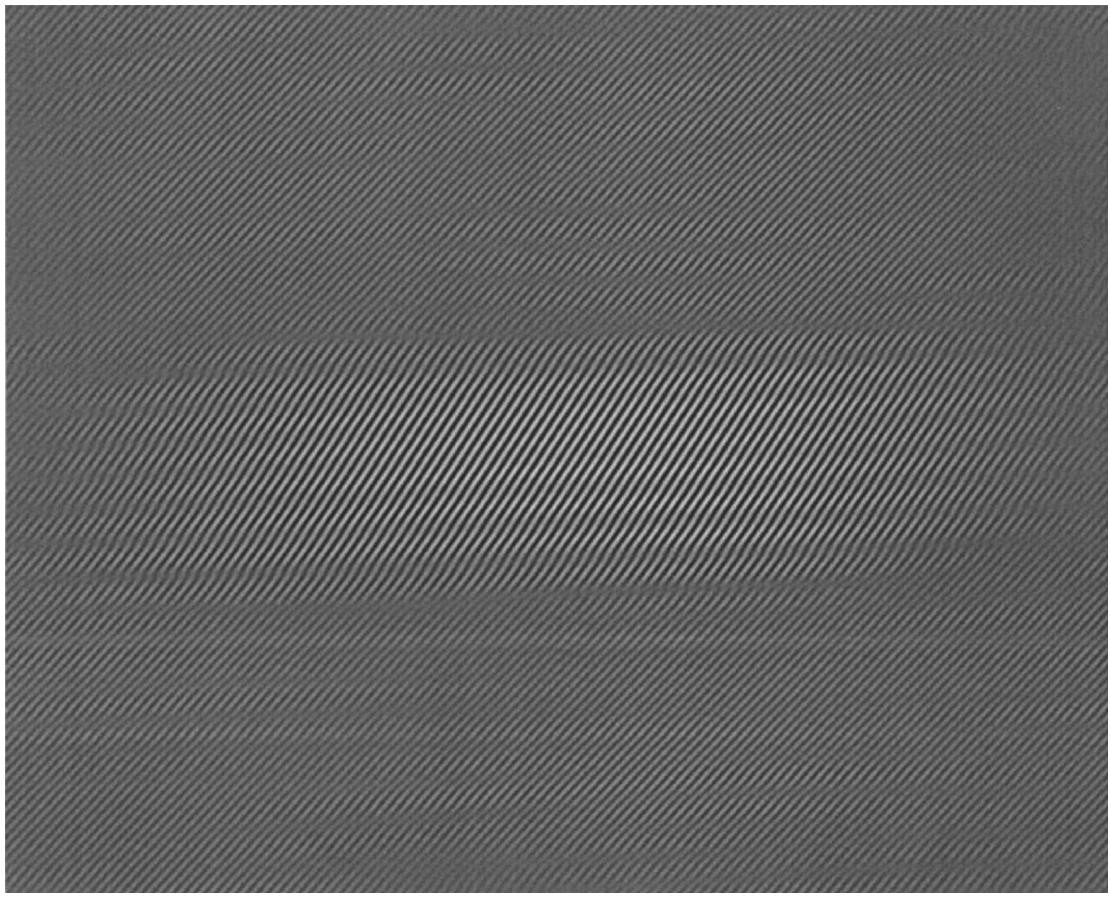

Figure 20 Reconstructed image from Fourier transformation of precipitate in peak aged Cu-0.7%Cr-0.3%Fe alloy. Precipitate appears partially coherent with the copper matrix.

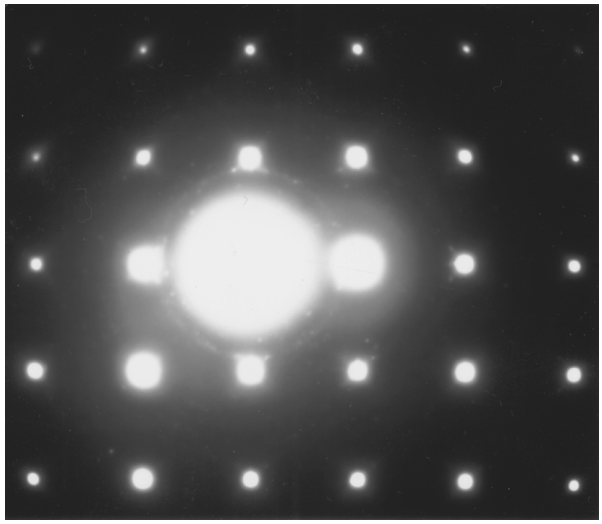

Figure 21 Diffraction pattern of overaged Cu-0.7%Cr-0.3%Fe alloy. Rings are still visible as are faint ordered reflections. Beam direction B = [1, 0, 0].

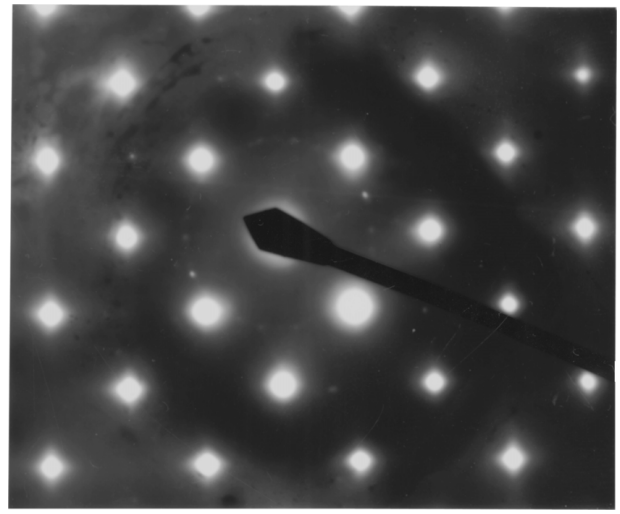

Figure 23 Diffraction pattern of peak aged Cu-0.7%C-0.8%Fe alloy. Additional reflections due to incoherent precipitates are visible. Beam direction B = [1, 0, 0].

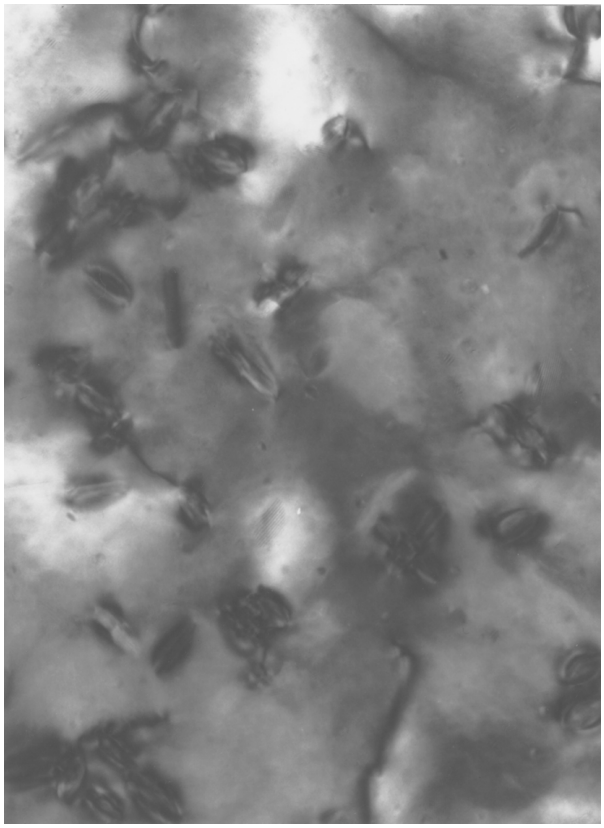

Figure 22 TEM bright field image of peak aged Cu-0.7%Cr-0.8%Fe alloy showing rod like precipitates between 30–50 nm in length. Beam direction B = [1, 0, 0]. 100 k.

3.6.5. Peak aged Cu-0.7%Cr-0.8%Fe and Cu-0.7%Cr-2.0%Fe

Microstructures of peak aged Cu-0.7%Cr-0.8%Fe (Alloy B) and Cu-0.7%Cr-2.0%Fe (Alloy C) alloys were also investigated. Both alloys were aged at 600°C for 1 hour. The precipitates in Alloy B were observed to be randomly oriented and had a morphology similar to those of peak aged Alloy A as shown in Fig. 22. The precipitates were considerably larger, 30–50 nm in length. Fig. 23 shows a diffraction pattern from the sample. A diffraction ring can be seen in addition to many other random reflections, caused by the precipitates. These indicate that the precipitates are not coherent. More rings were not seen presumably because the precipitates were too coarse. Indexing of the one ring showed that it was equivalent to the most intense ring seen in the diffraction patterns of Alloy A. This indicated that the precipitates were also bcc.

The microstructure of the peak aged Alloy C was found to contain very high concentrations of precipitates. The morphology of the precipitates was quite different to that of the other two alloys as shown in Fig. 24. Here the precipitates appeared spherical. The diameter of the precipitates was between 30–40 nm. Diffraction patterns showed that precipitates were randomly oriented indicating they were not coherent. Fig. 25 shows many additional reflections due to precipitates, far more than seen in Alloy B indicating a greater concentration of precipitates. Coarse rings could be seen however they were not continuous, presumably due to the size of the precipitates. Indexing of rings produced the same results as that for Alloy A indicating precipitates have a bcc crystal structure.

EDS was carried out on precipitates in the peak aged Alloy C during the TEM investigation of the microstructure. A very small spot size was used to try to improve the accuracy of measurements. Fig. 26 shows a spectra obtained from the matrix, Fe and Cr peaks are visible. A typical spectra taken from the Cr rich eutectic phase is shown in Fig. 27. Both Fe and Cr are present in approximately the same proportions. A typical spectra obtained from a secondary precipitate is shown in Fig. 28. Precipitates contained both Fe and Cr however in comparison to the spectra of the Cr rich eutectic phase it was apparent that the amount of Fe in the secondary precipitate was considerably higher. These results were in general agreement with those observed during the EDS analysis of precipitates in the AC condition using the scanning electron microscope. Further comparison of spectra was not possible due to the different conditions under which they were obtained.

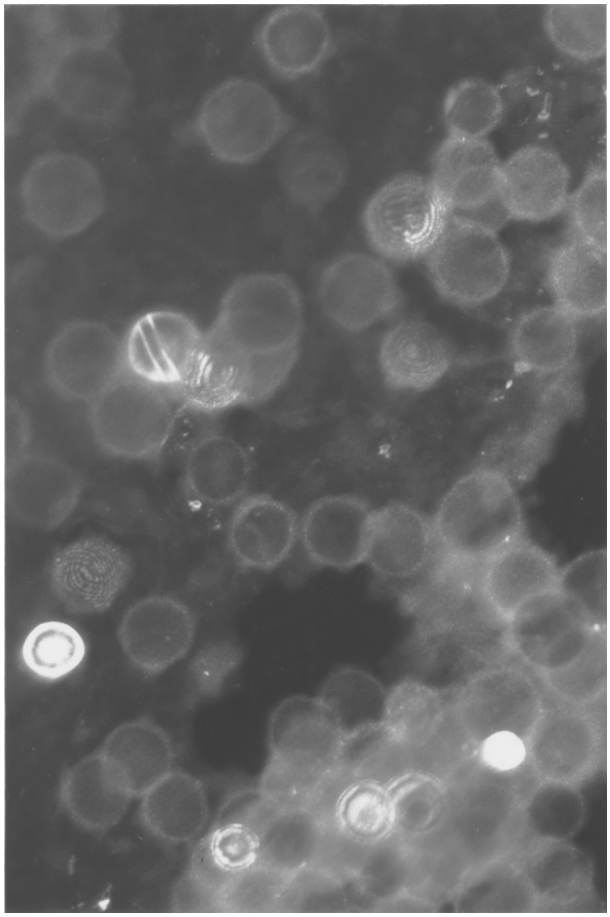

Figure 24 TEM dark field image of peak aged Cu-0.7%Cr-2.0%Fe alloy showing large spherical precipitates, between 30–40 nm in diameter. Beam direction B = [1, 0, 0]. 100 k.

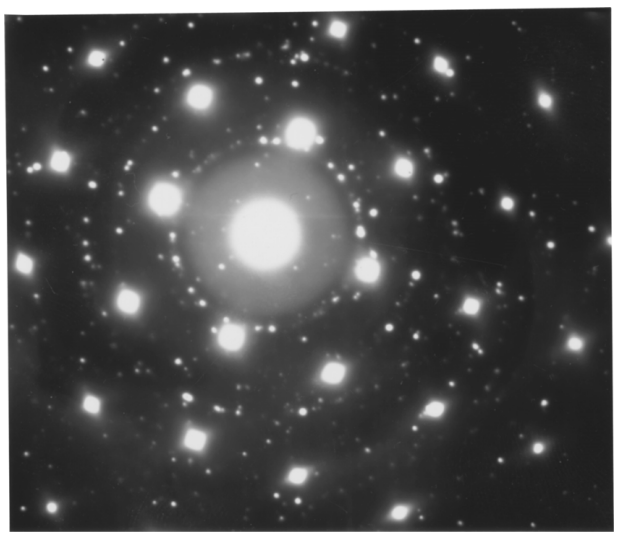

Figure 25 Diffraction pattern of peak aged Cu-0.7%C-2.0%Fe alloy. Additional reflections and semi-continuous rings due to incoherent precipitates are visible. Beam direction B = [1, 0, 0].

3.7. Summary of microstructural characterisation

Optical and scanning electron microscopy showed that the microstructure of each alloy was dendritic. Eutectic surrounded the dendrites in each alloy except for the Cu-1%Fe alloy. The grain size of each alloy was large and would be expected to have very little effect on the mechanical properties.

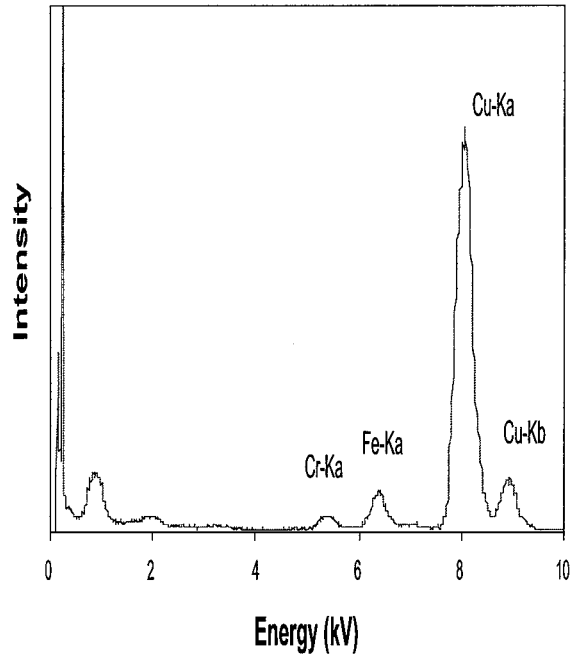

Figure 26 EDS spectra from matrix of peak aged Cu-0.7%Cr-2.0%Fe alloy obtained during TEM investigation.

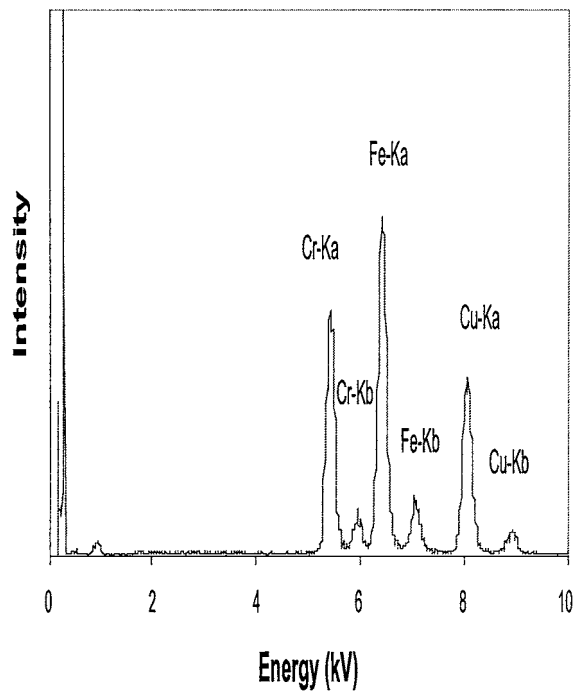

Figure 27 EDS spectra from primary precipitate of peak aged Cu-0.7%Cr-2.0%Fe alloy obtained during TEM investigation.

Results from EDS analysis showed that both primary and secondary precipitates contained Fe and Cr for each Cu-Fe-Cr alloy. The Fe/Cr ratio was dependant upon the alloy composition and the type of precipitate. WDS determined the concentration of Fe and Cr in the solution treated matrix of each alloy. Results showed that Fe and Cr reduced each others solid solubility. The solubility of Cr was found to be decreased more significantly.

The solution treated microstructure of Alloy A was observed to contain very few precipitates. After 5 minutes aging at 500°C considerable precipitation had occurred. The majority of precipitates were

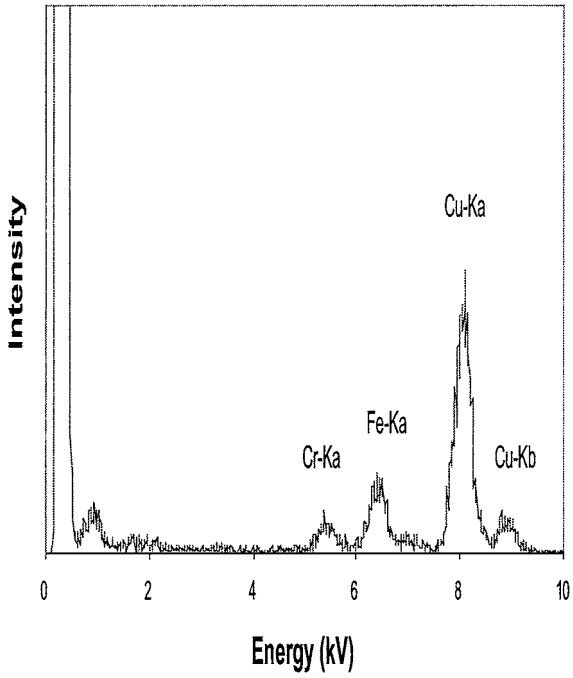

Figure 28 EDS spectra from secondary precipitate of peak aged Cu-0.7%Cr-2.0%Fe alloy obtained during TEM investigation.

randomly oriented based upon the diffraction rings in the diffraction pattern and hence appeared to be incoherent with the copper matrix. The microstructure of the peak aged alloy contained a high concentration of precipitates which appeared to be rod shaped. Precipitates were between 10 and 20 mm long, only marginally larger than those observed in the specimen aged for 5 minutes. Diffraction patterns from the peak aged sample contained clear diffraction rings. Indexing of the diffraction rings showed that the precipitates were bcc. Coarsening of the precipitates in the overaged alloy was not apparent from examination of the micrographs however diffraction patterns indicated coarsening had occurred.

High resolution lattice imaging on samples of peak aged Alloy A indicated that in addition to incoherent precipitates there were also some precipitates which were preferentially oriented with the copper matrix which indicated partial coherency. Evidence supporting this was found in diffraction patterns which showed faint ordered reflections surrounding (2, 0, 0) reflections of the matrix. These were in the same position as diffraction spots due to precipitates as seen in the diffraction patterns generated from high resolution micrographs of precipitates.

Examination of samples of the peak aged Alloy B showed that the precipitates had a morphology similar to those in Alloy A. Precipitates were considerably larger, between 30–50 nm long. Diffraction patterns indicated precipitates were randomly oriented and had a bcc lattice. Precipitates in the peak aged Alloy C had a different morphology from those of the other two Cu-Fe-Cr alloys. Precipitates were spherical and were about 30–40 nm in diameter. Diffraction patterns indicated that the precipitates were randomly oriented and had a bcc lattice structure. The random orientation reflected the incoherent nature of the precipitates with the matrix. EDS analysis in the TEM on secondary precipitates in Alloy C confirmed the precipitates consist of both Fe and Cr.

TABLE III Dimensions of secondary precipitates in peak aged Cu-Fe-Cr alloys

Alloy	Precipitates size range
Cu-0.7%Cr-0.3%Fe (Alloy A)	10 — 20 nm *
Cu-0.7%Cr-0.8%Fe (Alloy B)	30 — 50 nm *
Cu-0.7%Cr-2.0%Fe (Alloy C)	30 — 40 nm diameter

*length of rod.

The TEM showed that each of the Cu-Fe-Cr alloys contained secondary precipitates that were randomly dispersed in the copper matrix and as a result were considered to be incoherent with the copper matrix. Rings in diffraction patterns of each alloy indicated that precipitates were bcc. The size and morphology of secondary precipitates in the Cu-Fe-Cr alloys in peak aged condition were found to be dependant upon the Fe content of the alloy. The precipitates in Alloy A and Alloy B were rod shaped while those in Alloy C were spherical. The size range of precipitates in peak aged samples are summarised in Table III.

Evidence was also found to indicate the presence of preferentially oriented precipitates in Alloy A in all aged conditions.

4. Discussion

4.1. Mechanical properties

Isochronal and isothermal aging curves for the three solution-treated and aged Cu-Fe-Cr alloys showed that only the Cu-0.7%Cr-0.3%Fe alloy (Alloy A) had a significant age hardening response, which approached that of Cu-1%Cr (Alloy Z). The alloys Cu-1%Fe, Cu-0.7%Cr-0.8%Fe (Alloy B) and Cu-0.7%Cr-2.0%Fe (Alloy C) showed almost no age hardening response. Alloy C had a slightly higher hardness than Alloy B for all aging times. There were essentially the same trends for the 0.5% yield stress (σ_y). These trends can be explained by the microstructural characterisation.

Energy Dispersive X-ray Spectroscopy (EDS) of primary and secondary precipitates within the as-cast samples of the three Cu-Fe-Cr alloys showed that all precipitates contained both Fe and Cr. This was confirmed for peak aged Alloy C by the EDS spectra taken during the TEM investigation. Fe and Cr did not form separate populations of Fe and Cr precipitates but combined to form precipitates made up of Fe-Cr in solid solution in one another. In addition to Fe and Cr precipitates would be expected to contains some small fraction of Cu in solid solution. Evidence indicates that this is the case for all aged conditions. It is supported by the TEM results discussed later which show that the secondary precipitates in the three Cu-Fe-Cr alloys had a bcc crystal structure. It is not unexpected based upon:

1. The Fe-Cr phase diagram which shows that Fe and Cr have complete solid solubility in one another.

2. Results from the literature which show that neither Fe nor Cr form metastable intermediate precipitates when aged in Cu [4, 5].

The EDS spectra of the precipitates in the as-cast alloys indicate that the ratio of Fe to Cr is dependant upon the alloy composition. Moreover the ratio of Fe to Cr is different for primary (eutectic precipitates) and secondary precipitates in each alloy, primary precipitates contained a higher fraction of Cr. For both primary and secondary precipitates the ratio of Fe to Cr increased with alloy Fe content, ie. as the Fe content increased precipitates became richer in Fe. The increase was much more pronounced for the secondary precipitates.

The difference in composition of primary and secondary precipitates is related to their formation. The primary precipitates are formed during alloy solidification whereas secondary precipitates are derived from solid solution during cooling of the alloy. Wavelength Dispersive Spectroscopy (WDS) indicated that Fe and Cr decrease each others solubility in the Cu matrix. Table II shows that the amount of Cr in solid solution decreased from 0.55 to 0.51 to 0.40 wt% as the Fe content increased from 0.3 to 0.8 to 2.0 wt%. However for the Cu-0.7%Cr-0.3%Fe and Cu-0.7%Cr-0.8%Fe alloys almost all of the Fe dissolved into solid solution because the Fe concentration was far below the maximum solid solubility of Fe in Cu, 4.1 wt% [2]. The amount of Fe in solid solution in each alloy was 0.26, 0.78 and 1.60 wt%. Only for the Cu-0.7%Cr-2.0%Fe alloy (Alloy C) was the amount of Fe in solid solution significantly reduced by the Cr in solid solution. Because the Cr content of each of the three alloys was equivalent to the maximum solubility of Cr in Cu (0.73 wt% at 1076.2°C, to try and maximise precipitation hardening), the Fe in solid solution decreased the amount of Cr that was able to dissolve into solid solution. Instead the Cr formed Cr rich FeCr primary precipitates during solidification. In contrast, Fe rich FeCr secondary precipitates were formed on cooling from the solid solution.

For primary precipitates the increase in the ratio of Fe to Cr with increasing Fe was much less than for the secondary precipitates. Spectra taken from primary precipitates in Alloy A and B show very similar Fe and Cr peak heights, indicating essentially the same composition. WDS results show that increasing the Fe content decreases the solubility of Cr. This results in more Cr being available to form primary precipitates. This is balanced by the increase in overall Fe content of the alloy. However, because most of the Fe dissolves into solid solution, the results indicate that the ratio of Fe to Cr increases only slightly for the primary precipitates of the three alloys examined. Primary precipitates due to their size play essentially no part in the strengthening of these alloys; they are not discussed further.

Classical theory of precipitation hardening predicts that the peak strength is associated with a transition from precipitate cutting to precipitate looping. The transition is often associated with a loss of coherency of the precipitates. The size at which precipitates loose coherency is largely dependant upon the atomic mismatch between the precipitate and the matrix. The higher the atomic mismatch the smaller the precipitate size at which coherency is lost and the greater the strengthening as shown by the simplified Orowan looping equation [6]:

$$\Delta\sigma = 0.8Gb(f)^{1/2}/r \quad (1)$$

The atomic radius of bcc Cr is 1.249 Å, for fcc Fe 1.269 Å and for fcc Cu 1.278 Å [7]. For binary Cu-Cr and Cu-Fe alloys the higher atomic mismatch of Cr precipitates in Cu compared to that of Fe results in more misfit strain between the precipitate and matrix. This is reflected in the morphology of the precipitates. Discs are nucleated when the misfit strain is $\geq$5% whereas spheres are formed when the strain is $\leq$3% [8]. Weatherley *et al.* [9] reported needle shaped Cr precipitates in Cu-Cr, whereas spherical Fe precipitates have been reported by Saji *et al.* [10] and Hirato & Kano [11] in binary Cu-Fe systems. Due to the higher misfit strain a finer distribution of precipitates are nucleated and coherency between the precipitate and the matrix is lost at a finer precipitate size. This means that the transition from the cutting to the looping mechanism occurs at a finer precipitate size than for Cu-Fe resulting in more precipitation hardening. For a Cu-0.94wt%Cr alloy, the precipitate size in the peak aged condition has been reported to be 10 nm [5] compared to values between 35 and 70 nm for binary Cu-Fe alloys [10]. The difference in misfit strain between Fe and Cr precipitates is the primary reason for the larger age hardening response of Cu-Cr alloys in comparison to Cu-Fe alloys.

The results of EDS and WDS analysis suggested that precipitates in the Cu-Fe-Cr alloys were made up of a solid solution of Fe and Cr. The ratio of Fe to Cr in the secondary precipitates increased as the Fe content of the alloys increased. Based upon the peak aged precipitate sizes of the binary Cu-Fe and Cu-Cr alloys, an increase in precipitate size would be expected as the ratio of Fe to Cr increased. Similarly this is expected based upon the theory of precipitation hardening and the properties observed for the three Cu-Fe-Cr alloys investigated, ie increasing Fe content, decreased age hardening response.

This was confirmed in the TEM investigation of microstructures of each of the Cu-Fe-Cr alloys. Micrographs of the three Cu-Fe-Cr alloys in the peak aged condition showed that the precipitates increased in size and changed morphology with increasing Fe content. Precipitates in Alloy A and Alloy B were both rod shaped in the peak aged condition. Rods were between 10 and 20 nm long in Alloy A and between 30 and 50 nm long in Alloy B. This is similar to the results of a number of authors who have reported needle, lath and rod shaped precipitates in binary Cu-Cr alloys [9, 12–14]. For Alloy C, the precipitates were spherical with a diameter between 30 and 40 nm. Spherical precipitates have been reported in binary Cu-Fe alloys by Saji *et al.* [10] and Hirata & Kirano [11]. From this it is apparent that as the Fe content of the alloys increases, not only does the Fe content of the secondary precipitates increase, but also their morphology changes from that

observed in binary Cu-Cr alloys to that of binary Cu-Fe alloys. This is reflected in the age hardening responses of the three alloys.

TEM results show that as the Fe content increases, the size of the precipitates in the peak aged condition increases. The mechanism for this has been explained using results from EDS and quantitative WDS. As the precipitate size increased, the size of the age hardening response decreased in accordance with precipitation hardening theory. Further work is required in order to explain the inter-relationship between misfit strain and the composition and crystal structure of the secondary precipitates. The marginally higher HV and σ_y of Alloy C compared to Alloy B for all aged conditions (despite the smaller age hardening response for Alloy C) is attributed to the higher content of Fe in solid solution resulting in more solid solution strengthening. Evidence from quantitative microanalysis and conductivity tests support this assertion.

4.2. TEM

In the above section, the size of secondary precipitates in the peakaged condition, as determined from TEM, were discussed and used to explain the differences in aging responses of the three Cu-Fe-Cr alloys. In this section TEM results are used to interpret the precipitation reaction in the Cu-Fe-Cr alloys.

TEM analysis was carried out on the microstructure of Alloy A in the solution treated, the under aged, the peak aged and the over aged condition. Alloys B and C were investigated in the peak-aged condition. Examination of solution treated micrographs of Alloy A showed that some precipitation had occurred during quenching. Similar results have been reported for binary Cu-Fe alloys [4, 15] and Cu-Cr alloys [16, 17]. In contrast there was no evidence of precipitates in the diffraction pattern taken from the matrix of the solution treated alloys. The reason for this is thought to be that the volume fraction of precipitate was too low.

Micrographs of underaged Alloy A showed that considerable precipitation had occurred after 5 minutes aging at 500°C. The low equilibrium solid solubility of Cr in Cu at this temperature means that there is a large driving force for precipitation. A fine dispersion of precipitates was formed. Both Cu-Fe and Cu-Cr alloys are hardened directly by the equilibrium precipitate which forms from solid solution [14, 18–20]. Precipitates are initially coherent with the matrix but become semi-coherent and finally incoherent as they increase in size with aging. Since it has been shown that precipitates in the alloys investigated are solid solutions of Fe and Cr the same precipitation sequence is expected for all alloys.

Micrographs showing the development of precipitates with ageing time did not indicate a significant increase in precipitate size. This data is summarised in Table IV.

These result are consistent with the age hardening curve for Alloy A which showed a rapid increase in hardness with short aging times followed by a broad hardness peak and a gradual softening with prolonged exposure. The rapid increase in hardness with short aging time is attributed to a rapid and large amount of precipitate formation due to the large thermodynamic driving force for precipitation. The broad hardness peak is attributed to the precipitates having a wide distribution of sizes as evident in the high resolution images of the microstructures. The wide distribution of precipitate sizes suggests that the critical size for maximum hardening is not reached by all precipitates at the same time.

TABLE IV Range of precipitate sizes observed in TEM investigation of the microstructure of the Cu-0.7%Cr-0.3%Fe alloy in different aged conditions

Condition	Age Time	Precipitate Size
Under Aged	5 min 500°C	5 — 20 nm
Peak Aged	180 min 500°C	10 — 20 nm
Over Aged	720 min 500°C	10 — 20 nm

More information about the precipitation reaction in Alloy A was revealed by the diffraction patterns. The diffraction pattern of the solution treated alloy showed no sign of secondary precipitates other than some diffraction spots elongated along the ⟨2, 2, 0⟩ direction. The diffraction pattern of the specimen aged for 5 minutes contained faint semicontinuous rings. These rings indicated that the precipitates were randomly oriented and were thus not coherent with the matrix. In the peak aged diffraction patterns the diffraction rings were much more pronounced indicating that the volume fraction of secondary precipitates had increased. In addition to the rings in the diffraction pattern, there were reflections arranged periodically around the matrix reflections. These indicated that some of the precipitates were preferentially oriented with the matrix. Diffraction patterns taken from high resolution images of the precipitates further indicated that precipitates in the matrix were semicoherent. Close examination of the diffraction pattern of the underaged sample, reveals faint reflections arranged around the lattice reflections in the same patten as those seen in the peak aged samples. In diffraction patterns from the overaged sample the rings were no longer as clear or as continuous as those in the peak aged sample. This indicated that the precipitates had coarsened and the total number had decreased. Ordered reflections could still be seen around the major lattice reflections indicating that even in the overaged condition, the partial coherency of the precipitates had not been lost completely. Similar results have been reported by Hall and Aaronson [21] for overaged Cu-0.3%Cr.

Indexing of diffraction rings in each of the diffraction patterns showed that the secondary precipitates had a bcc crystal structure. The positions of lattice diffraction peaks are almost identical for bcc Fe and Cr ie. it is not possible to tell Cr and Fe precipitates apart by indexing of diffraction patterns. Precipitates consisting of a bcc solid solution of Fe and Cr would produce the same diffraction rings as those observed. Results were supported by X-ray diffraction scans from overaged samples of Alloy A which showed faint diffraction

peaks in positions corresponding to bcc precipitates of Cr and Fe. Diffraction patterns from high resolution images of precipitates showed that the lattice spacing of precipitates were approximately 2.02 Å, equivalent to the lattice spacing of (1, 1, 0) planes in both bcc Fe and Cr. The bcc crystal structure of the precipitates in all aged conditions for Alloy A is in agreement with results reported for binary Cu-Cr alloys [9, 13, 21].

Precipitates have been shown to consist of a solid solution of Fe and Cr. The TEM analysis shows that the secondary precipitates are bcc. Based upon the present work and the evidence available in literature on the precipitation reactions of Fe and Cr alloys, no intermediate precipitates are believed to form in the three Cu-Fe-Cr alloys. The equilibrium bcc precipitates are thought to be directly responsible for hardening. Results indicate that the precipitates lose coherency with the copper matrix after short aging times. Diffraction patterns from the sample aged for five minutes at 500°C show that most of the precipitates were not coherent with the copper matrix as evidenced by the diffraction rings. With further aging these precipitates coarsened. Diffraction patterns from the peak aged sample contained both rings and ordered diffraction spots. These indicate some of the precipitates may be semi-coherent with the matrix in the peak aged condition. High resolution images indicated precipitates were rod shaped and 10–20 nm long. With continued aging, further coarsening of the equilibrium precipitates occured and the level of coherency would be expected to decrease ie, precipitates go from semicoherent to incoherent. Little evidence of precipitate coarsening was observed in high resolution images of the overaged matrix; however diffraction patterns indicated that the amount of precipitate coherency had decreased and that some precipitate coarsening had occurred.

The microstructures of peak aged samples of Alloy B and Alloy C were investigated using TEM. The precipitation reaction of these two alloys are expected to be the same as that of Alloy A. The morphology and size of the secondary precipitates in peak aged Alloy B and C have already been discussed in relation to the mechanical properties observed. The diffraction pattern of Alloy B showed only one faint discontinuous diffraction ring and some random reflections. Indexing of the ring showed it to be equivalent to the most intense ring seen in Alloy A, and indicated that the precipitates were bcc. The discontinuity of the diffraction ring compared to those for Alloy A is attributed to the increased size of the randomly oriented precipitates as was seen in bright field images of the microstructure. No evidence of ordered reflections could be seen in the diffraction pattern. The bright field images of Alloy C contained a high volume fraction of large spherical precipitates. This is reflected in the diffraction pattern which contains numerous random reflections and coarse discontinuous rings. The high volume fraction of precipitates in this alloy compensates for the increased precipitate size compared to Alloy A and B. Indexing of rings showed the precipitates to be bcc. As for Alloy B there was no evidence of ordered reflections, indicating that peak hardness in Alloy B and Alloy C (which contain larger precipitates in peak aged condition) occurs when precipitates become incoherent with the copper matrix.

Results of TEM analysis have shown that precipitates in each of the alloys are bcc. Each of the three Cu-Fe-Cr alloys are hardened by equilibrium bcc precipitates. The different peak aged mechanical properties can be related to the different peak aged precipitates sizes. Precipitation in Alloy A occurs rapidly followed by a slow coarsening of the precipitates as reflected in the age hardening curves. The precipitates in Alloy A have a similar morphology to those reported for binary Cu-Cr alloys. Results show that some precipitates are preferentially oriented within the matrix in the peak aged condition indicating that they are semicoherent.

4.3. Mechanical properties and the Orowan equation

As has been discussed, classical precipitation hardening theory suggests that peak aged mechanical properties are associated with a transition from particle cutting to particle looping at a critical precipitate size and dispersion. The Orowan equation predicts the amount of strengthening caused by dispersions of precipitates that are not sheared by dislocations and can therefore be applied to predict the amount of strengthening due to secondary precipitates in the peak aged condition. The original Orowan equation was modified into the Orowan-Ashby equation [22]:

$$\Delta\sigma = 0.84MGb/2\pi(1-\nu)^{1/2}L * \ln r/b \quad (2)$$

where M is the Taylor factor ($\cong$3), G is the shear modulus of the matrix, b is the matrix Burgers vector, r is the particle radius, ν is the Poisson ratio of the matrix and L is the average interparticle spacing. This equation has been widely used to model the behaviour of dispersion strengthened copper alloys [23, 24]. It is important to note that the Orowan-Ashby equation assumes precipitates are spherical, have uniform size and strength and are distributed uniformly within the matrix. The effective average interparticle spacing (L) was calculated using the equation:

$$L = \pi^{1/2} * r_s/f^{1/2} \quad (3)$$

Where r_s is planar particle radius given by $r_s = (2/3)^{1/2} * r$, r is the average particle radius and f is the volume fraction of precipitate. This equation was developed by Brown & Ham [25] and applies to systems in which the Orowan mechanism operates. The value of L can be further refined by taking into account the finite size of the precipitates [25]:

$$L_{\text{final}} = L - 2r_s \quad (4)$$

This is the value that was used in the calculation of the Orowan-Ashby Equation.

From the results of the TEM analysis on each of the peak aged alloys, the amount of strengthening observed can be compared to that predicted by the Orowan-Ashby equation. A number of assumptions have had to be made in order to do this. The average particle size

of each of the alloys used in the equation is half that of the range observed in the bright field images of the microstructure. For Alloy A and B precipitates were observed to be rods as opposed to spheres, in the calculations they were considered to be spherical. The volume fraction of precipitate in each of the three alloys was calculated based upon the solution treated WDS results and the results of resistivity testing used to determine isotherms of the phase diagram. For each alloy the volume fraction of precipitates was calculated after first subtracting the concentration of alloying elements in solid solution at the aging temperature, as calculated by resistivity results, from that of the solution treated WDS results. For each of the alloys the values of G, b and ν used in the equations were those of Copper. This was thought acceptable as conductivity and isotherm results had shown that the concentration of Fe and Cr in solid solution in the peak aged condition was very low. The values used in the calculation are shown in Table V.

The values calculated using the Orowan-Ashby equation for the increase in yield stress due to the secondary precipitates are shown in Table VI. The Orowan-Ashby equation predicts the same trends as determined from experimental results, however there is some difference between the amount of strengthening predicted and the actual yield stress recorded for the alloys. When the increase in yield stress predicted by the Orowan-Ashby equation is added to that of the matrix material, 26 MPa [29], the agreement between calculated and actual values is reasonable. Note that the yield stress for the matrix material used is that of a single crystal of copper so as to include no grain boundary strengthening.

These results indicate that the effect of primary precipitates, grain boundary strengthening and solid solution strengthening upon the yield stress (σ_y) of the peak aged alloys is minimal. This is as expected based upon the results of the characterisation.

TABLE V Values used to determine the amount of strengthening due to the Orowan mechanism

Value	Alloy A	Alloy B	Alloy C	Reference
R (nm)	7.5	20	17.5	—
L (nm)	103	219	149	—
M	3	3	3	Ardell [26]
G (GN/m^2)	46.8	46.8	46.8	Amer. Inst. Physics. Hand book [27]
ν	.308	.308	.308	″
B (nm)	.256	.256	.256	Ashby & Jones [28]

TABLE VI Increases in yield stress calculated using the Orowan-Ashby equation and data determined from TEM analysis of peak aged microstructures

Alloy	$\Delta\sigma_{\text{Orowan}-\text{Ashby}}$	σ_y	$\Delta\sigma_{\text{Orowan-Ashby}} + \sigma_{\text{matrix}}$
Alloy A	189	288	215
Alloy B	115	122	141
Alloy C	164	135[1]	190

[1]For Alloy C, peak yield stress was recorded in the solution treated condition. The yield stress reported is that of Alloy C after having been aged for a time equivalent to that of the TEM specimen from which data for the calculation was collected.

Optical metallography of the as-cast microstructures of the three Cu-Fe-Cr alloys had shown that the microstructure of each alloy was dendritic with a rod like eutectic having formed around dendrite arms. Primary precipitates within the eutectic were of the order of μm. The effect of precipitates of this size upon the σ_y would be minimal.

The effect of the observed grain size upon the yield stress was calculated using the Petch equation. It was calculated that the increase in yield stress due to the equiaxed grains for Alloy C was of the order of 16 MPa. For the larger columnar grain sizes for Alloys A & B the amount of strengthening was negligible.

Similarly, the effect of solid-solution strengthening upon the yield stress of these alloys in the peak aged condition, relative to the effect of precipitates, would be minimal. Results of resistivity testing have shown that, at the ageing temperatures of these alloys, the concentration of Fe and Cr in solid solution is low. The amount of solid solution strengthening would therefore be low as indicated by the results.

Based upon the results of the characterisation it is apparent that the Orowan-Ashby equation predicts the peak aged yield stress of the three alloys investigated with a reasonable degree of accuracy. This indicates that the peak aged mechanical properties are associated with a transition from particle cutting to looping for three Cu-Fe-Cr alloys investigated. A closer fit between experimental and predicted properties would be expected if more quantitative data was used for the modelling. The collection of more quantitative date is a subject for further research. Results that support peak mechanical properties being associated with a transition from particle cutting to looping have been reported for equivalent copper systems by Matsuura *et al.* [30], Rotem *et al.* [31], Miyake & Fine [23] and Anderson *et al.* [24]. Present results are in agreement with these previous studies.

4.4. Electrical properties

Conductivity testing on the three solution treated and aged Cu-Fe-Cr alloys showed that the peak aged electrical conductivity (δ) of the three Cu-Fe-Cr alloys was dependant upon the Fe content. Peak aged conductivities, based upon the aging times where peak hardness occurred, were: Alloy A - 69% IACS, Alloy B - 64% IACS and Alloy C - 54% IACS. The lower δ of Alloy C is partly a result of the higher aging temperature of 600°C as opposed to 500°C used for Alloy A and B (higher equilibrium solubility of Fe and Cr), but more important is the higher Fe content. After aging for 360 minutes the conductivities were, 75, 64 and 57% IACS for alloys A, B and C.

WDS measurements of solution treated samples have shown that Fe and Cr have a negative effect upon each others solubility in copper. Due to the compositions of the alloys being investigated (ie, Cr content near its solubility limit in copper for each alloy) the amount of Fe in solid solution after aging increases and the amount of Cr decrease as the Fe content of the alloys increases. This is reflected in the isotherms determined for the

Cu rich corner of the Cu-Fe-Cr ternary phase diagram. From literature it is known that Fe in solid solution is more detrimental to the electrical conductivity (δ) of Cu than Cr [32]. Therefore as the Fe content of the alloys increases, the amount of Fe in solid solution after aging increases and δ decrease as is reflected in the present results.

As has previously been discussed, there is a high driving force for precipitation in each of the three Cu-Fe-Cr alloys. The conductivities of the three Cu-Fe-Cr alloys in the solution treated condition were very close; Alloy A - 26% IACS, Alloy B - 27% IACS & Alloy C- 28% IACS. A greater decrease in solution treated δ was expected based upon the increasing alloy content. This was attributed to little precipitation having occurred during quenching. Similarly, for each of the solution-treated alloys, δ rapidly increased after very short aging times. For each alloy, in excess of 60% of the final overaged δ was reached after twenty minutes of aging at 500°C. This was due to a rapid decrease in the concentration of alloying elements in solid solution as proven by the amount of precipitation that had occurred after five minutes aging in Alloy A. The rate at which δ increased for Alloy A was significantly higher than that of either Alloy B or C. This was attributed to the slower precipitation kinetics of Fe in comparison to that of Cr, ie. as the Fe content in solid solution increased the rate of precipitation of secondary Fe-Cr precipitates decreased. The kinetics of precipitation would be determined by the degree of thermodynamic metastability. Since Cr has a much lower equilibrium solubility than Fe it is expected that the solution treated condition for Cu-Cr represents a higher state of metastability, therefore precipitation would occur at a much higher velocity in comparison to solution treated Cu-Fe alloy. This is supported by literature results which indicates that the precipitation kinetics of Cu-Fe alloys are very slow [33].

In order to calculate the amount of strengthening due to secondary precipitates using the Orowan Ashby equation, it was necessary to calculate the interparticle spacing (L) using Equation 3, $L = \pi^{1/2} r / f^{1/2}$. This equation was not suitable to calculate the distance between precipitates in regard to their possible effect upon conductivity. The reason is that the equation calculates the interparticle distance between precipitates when the Orowan mechanism is operating. The interparticle distance calculated is effectively the number of precipitates per unit length of dislocation where the dislocations are not straight lines but are curved around and between the precipitates. Instead equation:

$$L = r / f^{1/2} \tag{5}$$

was used as it calculates the straight line distance between precipitates assuming all precipitates are spherical, the same size and are arranged in a repeating square array [25]. This is a more accurate approximation of the interparticle distance as experienced by conducting electrons in the copper matrix because electrons travel in straight lines between scattering events.

Calculated values of L are shown below in Table VII. It is apparent that the interparticle distance in each of the alloys is >42 nm (the mean free path of electrons in copper [34]), which in the literature [34] was reported to be the limit below which precipitates begin to significantly hinder the flow of electrons through the copper matrix and lower the conductivity (δ). The actual mean free path of electrons in the three Cu-Fe-Cr alloys would be significantly lower than 42 nm due to Fe and Cr atoms in solid solution. The effect of precipitates upon the δ would therefore be insignificant. Results of Miyake and Fine [23] support this view. Similarly, the grain size of each of the alloys was very large, and minimal scattering of conduction electrons would occur from the grain boundaries. Based upon this and the measured conductivity data, it is apparent that the δ of the alloys is determined predominantly by the concentration of alloying elements in solid solution after aging, the amount of which is dependant on the initial composition of the alloy and the aging temperature.

TABLE VII Interparticle distance calculated using Equation 5 and data collected from TEM analysis of peak aged microstructures

Alloy	Interparticle Distance (L)
Cu-0.7%Cr-0.3%Fe (Alloy A)	75 nm
Cu-0.7%Cr-0.8%Fe (Alloy B)	175 nm
Cu-0.7%Cr-2.0%Fe (Alloy C)	123 nm

4.5. Summary of iterpretation of results

From the results, it was apparent that as the Fe content of the alloys increased so the mechanical and electrical properties approached the properties of the Cu-1%Fe reference alloy. Fe additions were seen to decrease both the peak aged conductivity and the size of the age hardening response compared to that of the Cu-1%Cr alloy. In the peak aged condition the hardness and electrical conductivity of Alloy A were 148 HV and 74% IACS compared to 164 HV and 81% IACS for the reference Alloy Z.

The reason for the decrease in mechanical properties was shown to be that Fe and Cr do not form separate populations of precipitates. Precipitates in the three Cu-Fe-Cr alloys are made up of a solid solution of Fe and Cr. Alloys are believed to be hardened directly by the equilibrium precipitate. As the Fe content of the alloy increased so to did the concentration of Fe in the secondary precipitates. As a result, the precipitates became more like those of copper rich Cu-Fe alloys than Cu-Cr alloys as evidenced by the increase in the precipitate size in the peak aged condition and the change in precipitate morphology from rods to spheres. As a result, mechanical properties became more like those of Cu-Fe and less like Cu-Cr, ie had a decreased age hardening response.

The electrical conductivity (δ) similarly decreased as the concentration of Fe increased. The reason for this was that, as the Fe content increased, so too did the concentration of Fe in solid solution after aging. Plots of % IACS v aging time indicated that the rate of precipitation decreased as the Fe content of the alloys increased.

Results of TEM analysis indicated that secondary precipitates were bcc in each of the Cu-Fe-Cr alloys. The Orowan-Ashby equation was shown to reasonably predict the increase in yield stress due to the dispersion of secondary precipitates observed in the peak aged condition.

4.6. Comparison with existing commercial alloys

The investigation of alloys from the Cu rich corner of the Cu-Fe-Cr phase diagram explored the possibility of developing an alloy with a combination of properties equivalent or superior to those of existing, commercial, high-strength, high-conductivity (HSHC) alloys. The commercial copper alloys being targeted, based upon the compositions of the alloys being investigated, were precipitation hardened Cu-Cr alloys and cold-work stabilised Cu-Fe alloys. The two alloys with the most promising combination of properties were Cu-0.7%Cr-0.3%Fe and Cu-0.7%Cr-2.0%Fe.The properties would be expected to be improved by cold work and the influence of cold work is reported and discussed in a subsequent paper [35], however some of the conclusions of that work are included in the present discussion where relevant. The properties of the Cu-0.7%Cr-0.3%Fe alloy is discussed further in this paper.

The properties of the Cu-0.7%Cr-0.3%Fe alloy (σ_y, σ_{UTS}, hardness and electrical conductivity) approached but did not exceeded those of the Cu-1%Cr reference alloy. Peak aged properties of the Cu-0.7%Cr-0.3%Fe and Cu-1%Cr alloy are summarised in Table VIII, which includes the results after cold work [35].

Although the properties of Alloy A were not quite equal to those of Alloy Z, comparison of the cost of raw material to make the two alloys shows that Alloy A is ∼25% less expensive. This is illustrated in the cost comparison shown in Table IX. The reason is that Alloy A can be made using low carbon ferro-chrome as the source of chromium as opposed to Cu-Cr master alloy as is used industrially to make HSHC Cu-Cr alloys [36]. Ferro-chrome is less expensive than chromium because it can be produced directly from the mineral chromite without the necessity for any preliminary treatment to separate the iron and chromium [37]. The cost of raw materials used to calculate the cost per kg of alloy are shown in Table X.

It should be noted that in the cost comparison shown in Table IX, used the price for low carbon ferro-chrome quoted by the foundry alloy supplier, not that of the London Metal Exchange (LME). The reason being that because ferro-chrome is an alloying addition making up only 1 wt% of the alloy, it is unlikely that copper alloy manufactures would purchase sufficient quantities of ferro-chrome at a time in order to pay the lower LME rate. Ferro-chrome would be more likely purchased from foundry alloy suppliers. The conversion of LME prices for copper from $US to $A was done

TABLE IX Cost comparison of raw materials for producing 1 kg of Cu-1%Cr and Cu-0.7wt%Cr- 0.3wt%Fe alloy based upon prices listed in Table X

Alloy	Additions	Cost ($A)	Total ($A)
Cu-1%Cr	100 g Cu-10wt% Cr materalloy	0.1 * 9.20	0.920
	900 g Copper	0.9 * 2.12	*1.908*
			2.828
Cu-0.7%Cr-0.3%Fe	10 g Ferro-chrome	0.01 * 3.95	0.0395
	990 g Copper	0.990 * 2.12	*2.099*
			2.1385

TABLE X Material costs of raw materials for Cu-1%Cr and Cu-0.7%Cr-0.3%Fe alloys

MATERIAL	COST ($A/KG)	SOURCE
Copper	2.12	London Metal Exchange, average monthly spot price June, 1999
Low Carbon Ferro-Chrome	2.26	London Metal Exchange, average monthly spot price June, 1999
"	3.95	Price quoted, 1/6/99, by "Cast Metal Services," Foundry alloy suppliers, Brisbane, Australia
Cu-10wt%Cr Master-Alloy	9.20	Price quoted, 1/6/99, by "Austral Bronze Crane Copper, Ltd.," Sydney, Australia. Australian agent for "Affilips," Master-Alloy producers, Tienen, Belgium.

TABLE XI Ratios of yield stress and % IACS per Australian dollar for the Cu-0.7Cr-0.3%Fe and Cu-1%Cr alloys. Calculated using peak aged properties

	Cu-0.7%Cr-0.3%Fe		Cu-1%Cr	
Condition	σ_y/$A	% IACS / $A	σ_y / $A	% IACS / $A
Sol treat + aged	134	35	115	29
40%CW + aged	176	31	136	28
90%CW + aged	218	31	176	28

TABLE VIII Peak aged properties of Cu-1%Cr and Cu-0.7%Cr-0.3%Fe alloys in various aged conditions investigated

Alloy	Condition	Hardness (HV)	σ_y (MPa)	σ_{UTS} (MPa)	Cond (% IACS)
Cu-0.7%Cr-0.3%Fe	Sol treat + age 180 min 500°C	148	288	365	74
Cu-1%Cr	Sol treat + age 45 min 500°C	164	325	413	81
Cu-0.7%Cr-0.3%Fe	40%CW + age 90 min 450°C	165	377	460	67
Cu-1%Cr	40%CW + age 90 min 450°C	184	386	460	78.5
Cu-0.7%Cr-0.3%Fe	90%CW + age 90 min 450°C	171	467	537	66
Cu-1%Cr	90%CW + age 90 min 450°C	184	497	583	80.5

using an exchange rate of 1.51 $US to each $A. This was the average exchange rate over June, 1999.

Cu-Cr master alloys are used to make HSHC Cu-Cr alloys because of chromium's high oxidation rate. The recovery rate if pure chromium is added to the melt is low [36]. Experience indicates that this is not the case with additions of ferro-chrome. Castings carried out under atmospheric conditions indicated that excessive oxidation could be avoided if ferro-chrome was dissolved quickly into the melt. An oxide layer was seen to form on the surface of the melt; however the thickness of the layer was equivalent to that formed when Cu-1%Cr reference alloy was cast under the same conditions using Cu-10wt%Cr master-alloy. Problems with oxidation of alloying additions should be avoidable as it is standard practice when melting HSHC Cu-Cr and Cu-Fe alloys to use inert gas atmospheres or liquid slags to minimise the amount of oxidation [38–41].

The reason that ferro-chrome dissolved comparatively easily into the melt without excessive oxidation was believed to be because ferro-chrome is effectively a master alloy of 70 wt% Cr and 30 wt% Fe. The Cr is much more readily dissolved into solution than elemental chromium because the melting point of ferro-chrome, $\sim$1640°C [2] is significantly lower than that of chromium, 1875°C [2]. This was aided by the rapid dissolution rate which was achieved by the addition of fine pieces of ferro-chrome as opposed to large chunks. Initial difficulties with the slow dissolution rates of ferro-chrome in Cu due to the differences in the melting point, 1084°C compared to $\sim$1640°C were overcome by using very fine pieces of ferro-chrome (sieved through 2.5 mm screen) which increased the specific surface area of dissolving particles and therefore the dissolution rate within the copper melt. The increased rate of dissolution meant that there was less chance for oxidation of the Cr on the surface of the melt. It should be noted that communication with ferro-chrome suppliers within Australia indicates that ferro-chrome can be supplied in any size specification required by the customer without additional cost, ie. can be supplied as ferro-chrome fines.

Evidence suggests that the same casting techniques could be employed in the preparation of Cu-0.7%Cr-0.3%Fe alloys as currently used for casting other HSHC Cu-Cr alloys. Ferro-chrome additions could be made directly into the melt in place of Cu-Cr master alloys. Cost comparison shows that the raw materials are $\sim$25% cheaper. This is highlighted in Table XI.

Table XI shows that on a yield stress and % IACS per dollar basis the Cu-0.7%Cr-0.3%Fe alloy is more cost efficient than the Cu-1%Cr alloy. The low cost of Cu-Cr alloys is already one of the major reasons that they are so widely used in the electrical industry [42]. In light of this it is envisaged that there would be numerous applications for which HSHC Cu-Cr alloys are currently used, in both cast and wrought form, which could be replaced by less expensive Cu-0.7%Cr-0.3%Fe alloy made with low carbon ferro-chrome. Such applications include cable connectors, switch gears, circuit breaker parts, current carrying arms and shafts and resistance welding electrodes [43].

Comparison of the properties of alloy A to those of other commercial HSHC Cu alloys has shown that there is potential for this alloy to find commercial applications. The Cu-0.7%Cr-0.3%Fe alloy is an alternative to binary HSHC Cu-Cr for applications where some strength and electrical conductivity are required with economic advantage.

5. Conclusions

The aim of this project was to investigate the properties of copper rich Cu-Fe-Cr alloys for the purpose of developing a new cost effective, high strength, high conductivity copper alloy. Three alloys were initially selected for the investigation: Cu-0.7%Cr-(0.3, 0.8 and 2.0) %Fe. Two of these alloys have been shown to display unique sets of properties that could make them suitable for a range of commercial applications.

The Cu-0.7%Cr-0.3%Fe alloy displayed a combination of high strength and high conductivity, comparable to that of the commercial Cu-1%Cr alloy that is currently in extensive use. This was true in both cast and wrought form. The optimum combination of mechanical and electrical properties in the Cu-0.7%Cr-0.3%Fe alloy were obtained after ageing at 500°C for 45 minutes after solution heat treatment. Cold work of the solution treated alloy prior to ageing significantly improved the mechanical properties. A better combination of properties was obtained with 40% cold work prior to ageing compared to 90%. The optimum combination of properties were obtained for the 40% cold worked alloy after ageing for 90 minutes at 450°C. Cost modelling has shown that the new alloy is approximately 25% cheaper to produce than commercial Cu-1%Cr. It has also been shown to be more cost efficient on a yield stress and % IACS per dollar basis. The reason for the cost saving is that the Cu-0.7%Cr-0.3%Fe alloy can be made with low carbon ferro-chrome additions as the source of chromium rather than the more expensive Cu-Cr master-alloy. For applications in which cost is one of the primary materials selection criteria it is envisaged that there would be numerous applications in both cast and wrought form, where the Cu-0.7%Cr-0.3%Fe alloy would be more suitable than Cu-1%Cr.

Optical microscopy showed that the microstructure of each alloy was dendritic surrounded by a rod-like eutectic. The as-cast grain size of each alloy was in excess of 70 μm in all samples, the Hall-Petch equation indicated that the increase in yield stress that could be expected for this grain size was of the order of 16 MPa.

Energy dispersive X-ray spectroscopy (EDS) showed that the precipitates in all alloys consisted of both Fe and Cr. Composition was dependant on the initial composition of the alloy. Separate Fe and Cr precipitates were never observed. The ratio of Cr to Fe was higher for primary precipitates compared to secondary precipitates because of different modes of formation. The Fe content of the secondary precipitates increased as the Fe content of alloy increased.

Transmission electron microscopy (TEM) of the Cu-0.7%Cr-0.3%Fe alloy showed that the secondary precipitates had a body centred cubic (bcc) structure.

This was confirmed for peak aged Cu-0.7%Cr-0.8%Fe and Cu-0.7%Cr-2.0%Fe alloys. The size of the secondary precipitates in the peak aged samples of the three alloys increased with increasing Fe content. Precipitation hardening theory shows that the level of strengthening increases with decreasing peak aged precipitate size, this was confirmed with the results of the present work. The morphology of the precipitates was seen to change from that reported for binary Cu-Cr alloys to that reported for binary Cu-Fe alloys, ie. from rods to spheres, as the Fe content of the alloys was increased. EDS, wave-length dispersive spectroscopy(WDS) and TEM indicate that the equilibrium precipitate forms directly from solid solution in the ternary Cu-Fe-Cr alloys, similar to the precipitation reactions found in binary Cu-Fe and Cu-Cr alloys.

TEM analysis of the Cu-0.7%Cr-0.3%Fe alloy showed that there was a large driving force for precipitation, with a fine dispersion of precipitates observed after aging at 500°C for 5 minutes. Semi-continuous rings in the diffraction pattern indicated that precipitates were not fully coherent. With further aging, the rings in the diffraction pattern became continuous indicating that the precipitate volume fraction had increased. The secondary precipitates did not increase significantly in size with ageing; the length of the rod-shaped precipitates being between 5–20 nm after 5 minutes ageing, and between 10–20 nm in the peak aged condition (500°C). Ordered reflections in the diffraction patterns of the peak aged alloy indicated that some of the precipitates were preferentially oriented with the matrix. This was supported by high resolution images and diffractograms taken from the precipitates in the peak aged alloy which indicated that some precipitates were partially coherent with the matrix. No evidence of precipitate coarsening was seen in micrographs of overaged samples, but rings in diffraction patterns were less continuous indicating that precipitates had coarsened. Ordered reflections were still visible in the diffraction patterns of overaged samples, indicating that some precipitates were still preferentially oriented.

The results of TEM, WDS and resistivity measurements enable comparison of the increase in yield stress predicted by the Orowan-Ashby equation to that actually measured for the three ternary Cu-Fe-Cr alloys. This showed that the agreement between the amount of strengthening predicted by the theory and the measured strength was reasonable. These results support the accepted theory that peak aged mechanical properties in precipitation hardened systems is associated with a transition from particle cutting to dislocation looping.

The effect of adding chromium in the form of high carbon ferro-chrome instead of low carbon ferro-chrome was investigated for the Cu-0.7%Cr-0.3%Fe alloy. The mechanical properties of this alloy were found to be inferior to those of the same alloy made with low carbon ferro-chrome additions, because impurities such as C, S and P introduced with the high carbon ferro-chrome formed primary intermetallics with Cr and reduced the amount of Cr in solid solution.

It is clear that the properties of both the Cu-0.7%Cr-0.3%Fe and Cu-0.7%Cr-2.0%Fe alloy warrant further investigation. More detailed analysis of the optimum aging temperatures and times is required. Similarly further work is recommended in order to determine the optimum cold reduction prior to aging.

Acknowledgements

This work was supported by the Australian Research Council and by Copper Refineries Pty Ltd.

References

1. H. FERNEE, J. NAIRN and A. ATRENS, Precipitation Hardening of Cu-Fe-Cr Alloys, Part I, Mechanical and Electrical Properties, *J. Mater. Sci.* **36** (2001) 2711.
2. Metals Handbook, *Alloy Phase Diagrams*, ASM Handbook, vol. 3, 10th ed. (1990).
3. J. D. DONNAY, J. D. H. G. DONNAY, E. G. COX, O. KENNARD and M. V. KING, "Crystal Data: Determinative Tables," 2nd ed. (American Crystallographic Association (Publishers), 1963).
4. Z. BOJARSKI, W. BABINSKI, H. MORAWIEC, T. PANEK, J. RASEK and D. STROZ *Metals Technology* (1980) 248.
5. J. RYS and Z. RDZAWSKI, *ibid.* (1980) 32.
6. B. REPPICH, in "Materials Science and Technology - Plastic Deformation and Fracture of Materials," Vol. 6, edited by H. Mughrabi (VCH Publishers, New York, 1991) p. 311.
7. P. A. THORNTON and V. J. COLANGELO, "Fundamentals of Engineering Materials (Prentice-Hall, NJ, 1985).
8. J. W. MARTIN, in "Precipitation Hardening," edited by R. Robinson and D. A. Spihaus (Permangon, 1968).
9. G. C. WEATHERLY, P. HUMBLE and D. BORLAND, *Acta Metallurgica* **27** (1979) 1815.
10. S. SAJI, S. HORI and G. MIMA, *Transactions Japan Institute of Metals* **14** (1973) 82.
11. V. M. L. HIRATA and K. HIRANO, *Scripta Metallurgica* **31** (1994) 117.
12. Y. KOMEN and J. REZEK, *Metallurgical Transactions* **6A** (1975) 549.
13. N. J. LONG, C. H. LOYD and M. H. LORETTO, "Phase Transformations - Spring Review Course" (Institution of Metallurgists, 1979).
14. Z. RDZAWSKI and J. STOBRAWA, *Scripta Metallurgica* **20** (1986) 341.
15. A. BOLTAX, *Transactions AIME* **218** (1960) 812.
16. R. O. WILLIAMS, *Transactions of the ASM* **52** (1960) 530.
17. J. SZABLEWSKI and B. KUZNICKA, *Materials Science and Technology* **7** (1991) 407.
18. B. WINDOW, *Phil. Mag.* **26** (1972) 681.
19. F. HORNSTEIN and M. RON, *Acta Metall.* **22** (1974) 1537.
20. R. W. KNIGHTS and P. WILKES, *Metallurgical Transactions* **4** (1973) 2389.
21. M. G. HALL and H. I. AARONSON, *Acta Metall.* **34** (1986) 1409.
22. M. F. ASHBY, AIME Conference Proceedings, New York, Metallurgical Society AIME (Publishers), (1966) p. 143.
23. J. MIYAKE and M. E. FINE, *Acta Metall.* **40** (1992) 201.
24. R. K. ANDERSON, J. R. GROZA, R. L. DRESCHFIELD and D. ELLIS, *Metallurgical and Materials Transactions* **26A** (1995) 2197.
25. L. M. BROWN and R. K. HAM, in "Strengthening Methods in Crystals," edited by A. Kelly and R. B. Nicholson (Applied Science Publishers Ltd., London, 1971) p. 9.
26. A. J. ARDELL, *Metallurgical Transactions* **16A** (1985) 2131.
27. American Institute of Physics Handbook, 3rd ed. (McGraw-Hill, 1972).
28. M. F. ASHBY and D. R. H. JONES, "Engineering Materials 1: an Introduction to their Properties and Applications" 10th ed. (Butterworth Heinemann, London, 1995).
29. E. O. HALL, "Yield Point Phenomena in Metals & Alloys" (Plenum, NY, 1970) p. 38.

30. K. MATSUURA, M. KITAMURA and K. WATANABE, *Transactions JIM* **19** (1978) 53.
31. A. ROTEM, D. SHECHTMAN and A. ROSEN, *Metallurgical Transactions* **19A** (1988) 2279.
32. J. K. STANLEY, "Electrical and Magnetic Properties of Metals" (American Society of Metals (Publishers), Metals Park, Ohio, 1963).
33. R. E. WILLET, *Wire Journal*, Sept (1979) 124.
34. L. H. VAN VLACK, "Materials Science for Engineers" (Addison-Wesley, 1970).
35. H. FERNEE, J. NAIRN and A. ATRENS, Cold Worked Cu-Fe-Cr Alloys, *This Journal*.
36. Affilips, *Copper-Chromium Master Alloys*, Technical Data sheet no. 920119, produced by Affilips, Biezenstraat 27-31, B-3300, Tienen, Belgium (1994).
37. A. H. SULLY and E. A. BRANDES, "Chromium" (Butterworths, London, 1967).
38. Y. OHASHI, T. FUJINO, Y. TAKI and T. NISHIJIMA, US Patent no. 5,071,494 (1991).
39. E. ENCE, US Patent no. 3,640,779 (1972).
40. W. G. WATSON and J. F. BREEDIS, US Patent no. 4,224,066 (1980).
41. V. V. S. PRASAD, V. R. RAO, R. D. K. MISRA, P. KRISHNA RAO and K. M. GUPT, *Materials Science and Technology* **11** (1995) 1306.
42. J. J. CRONIN, *Metallurgical Engineering Quatro* **16** (3) (1976) 1.
43. Metals Handbook, "ASM Handbook," Vol. 2, 10th ed. (1990).

Received 25 April
and accepted 3 November 2000